DALTON

Preparation, structural and spectroscopic characterisation of the salts $M_3X_3AF_6$ (A = As or Sb, M = S or Se, X = Cl or Br) containing the novel sulfur– and selenium–halogen cations $(X_2MMMX)^+$ †

Scott Brownridge,[a] T. Stanley Cameron,[b] Jack Passmore,*[a] Gabriele Schatte[a] and Todd C. Way[a]

[a] *Department of Chemistry, University of New Brunswick, Fredericton, New Brunswick, E3B 6E2, Canada*

[b] *Department of Chemistry, Dalhousie University, Halifax, Nova Scotia, B3H 4J3, Canada*

The salts $X_2MMMX(AF_6)$ (A = As or Sb, M = S or Se, X = Cl or Br) were prepared quantitatively by the reaction of stoichiometric amounts of MX_3AF_6 and M or from stoichiometric amounts of M, X_2 and AsF_5 (M = S or Se; X = Br) in liquid SO_2. They have been characterised by elemental analysis, single-crystal X-ray diffraction, Fourier-transform (FT)-Raman and ^{77}Se FT-NMR spectroscopy. The crystal structures of $X_2MMMX(AsF_6)$ consist of $(X_2MMMX)^+$ cations and AsF_6^- anions. The structure of the $(X_2MMMX)^+$ cation is dominated by an intracationic halogen–chalcogen contact and M–M bond alternation giving rise to a short M–M bond distance indicative of thermodynamically stable np_π–np_π (n = 3 or 4) bonds. Since the structure of these cations is different from those of $(YM)_2MY^+$ (Y = Me or C_6F_5), theoretical calculations were performed to understand these differences and the bonding in these cations. In the $X_2SSSX(AsF_6)$ salts (X = Cl or Br) the structures of the cations are disordered and therefore exact bond distances could be not obtained. However, bond distances were estimated from their FT-Raman spectra and supported by molecular orbital calculations. The FT-Raman spectrum of $Se_2Br_5AsF_6$ is reported.

Various chalcogen cations of the type $M_aX_b^{x+}$ (M = chalcogen, X = univalent atom or group) in addition to MX_3^+ have been synthesised and structurally characterised over the last few years. The largest class of such compounds contains salts of sulfur– and selenium–iodine cations, although salts of SI_3^+ have not been prepared and stable neutral selenium and sulfur iodides are not isolable under ambient conditions.[1a] These include S_7IMF_6 (M = As or Sb),[1b] $(S_7I)_4S_4(AsF_6)_6$,[2a,c] $(S_7I)_2I(SbF_6)_3{\cdot}2AsF_3$,[2a,b] $S_2I_4(MF_6)_2$ (M = As or Sb),[3a] $Se_2I_4(AsF_6)_2{\cdot}SO_2$ and $Se_2I_4(Sb_2F_{11})_2$,[3b] SeI_3AsF_6,[4] $(Se_6I)_n(MF_6)_n$[5] and $Se_6I_2(AsF_6)_2{\cdot}2SO_2$[5] all of which were characterised by X-ray crystallography. The analogous less-stable S_7BrAsF_6[6] and $(S_7Br)_4S_4(AsF_6)_6$[6] have also been similarly characterised as well as $Se_2Br_5AsF_6$,[7] the iodine analogue of which is unknown. Other related structurally well characterised salts include $Te_6I_2(WCl_6)_2$,[8] $Se_6Ph_2(AsF_6)_2$,[9] $MeSSMe_2A$ (A = AsF_6 or $SbCl_6$),[10a,b,d,e] $MeS(SMe)_2AsF_6$,[10a] $MeS(SMe)_2SbCl_6$[10a,c] and $C_6F_5S(SC_6F_5)_2AsF_6$.[11a] Evidence has been presented for $C_2F_5Se(SeC_2F_5)_2Sb_2F_{11}$ and $(C_2F_5SeSeC_2F_5)_2(Sb_2F_{11})_2$.[11b] Except for MCl_3^+ (M = S or Se),[12,13] the only example of a sulfur/selenium chlorine cation to be unambiguously characterised is Se_9Cl^+,[14] although Raman evidence has been presented for the unstable S_7Cl^+ cation.[15] In addition, $S_2Cl_3^+$ and $Se_2Cl_3^+$ have been proposed in solution [16] and SCl^+ in the solid state.[17]

We report here the preparation and crystal structures of $S_3X_3AsF_6$, $Se_3X_3AsF_6$ and the preparation of $M_3X_3SbF_6$ (M = S or Se; X = Cl or Br) containing the first examples of $M_3X_3^+$ cations. The structures of the $(X_2MMMX)^+$ cations are of interest as they are the simplest unit in which several features found in the more complex halogeno–chalcogen cations are present: intracationic halogen–chalcogen contacts, and M–M bond alternation giving rise to short M–M bond distances indicative of thermodynamically stable np_π–np_π (n = 2 or 3) bonds. We have proposed that these features arise from positive charge delocalisation.[1a,18] The structure of the cations are also of interest as they are different from those of the related $M_3Y_3^+$ (Y = Me or C_6F_5) cations. In an attempt to understand these differences and the bonding in the chalcogen–halogen cations, extended Hückel (program CACAO),[19] MNDO (minimum neglect of differential overlap) and *ab initio* (GAUSSIAN: STO-3G*, LANL1DZ[20a] and 6-31G* basis sets)[20b] calculations were performed on $S_3H_3^+$, $S_3Cl_3^+$ and $Se_3Cl_3^+$ adopting different geometries. In addition, the structures of $M_3X_3^+$ in $M_3X_3AsF_6$ and $M_3X_3SbF_6$ (M = S or Se, X = Cl or Br) and the related $Se_2Br_5^+$ in $Se_2Br_5AsF_6$ were investigated by Fourier-transform (FT)-Raman spectroscopy. The nature of the $Se_3X_3^+$ cations in solution was studied by ^{77}Se FT-NMR spectroscopy. Preliminary accounts of part of this work have been published.[21,22]

Experimental

General procedures and reagents

All reactions were carried out in a one-piece apparatus consisting of two thick-walled round-bottom flasks (V = 25 cm^3) linked by a glass tube (outside diameter 10 mm) incorporating a sintered-glass filter disc (medium porosity). Both bulbs were fitted with Pyrex glass valves with poly(tetrafluoroethylene) (ptfe) pistons (J. Young, London, UK). Further details regarding general techniques and apparatus are described in ref. 23. All apparatus was carefully dried prior to use. Moisture-sensitive materials, crystals suitable for X-ray analysis and all solid products were manipulated in a Vacuum Atmospheres Dri-Lab equipped with a Dri-Train (HE-493) and an internal circulating drying unit containing 3 Å molecular sieves (1 kg). The FT-Raman spectra were obtained from neat samples sealed under a nitrogen atmosphere in thick-walled precision 5 mm NMR tubes (Wilmad Glass, Buena, NJ) on an FT-IR spectrometer (Bruker

† *Supplementary data available* (No. SUP 57126, 26 pp.): results of *ab initio* calculations and molecular orbital diagrams. See Instructions for Authors, *J. Chem. Soc., Dalton Trans.*, 1996, Issue 1.

Non-SI units employed: eV ≈ 1.60 × 10^{-19} J, E_h ≈ 4.36 × 10^{-18} J.

IFS66) equipped with a FT-Raman accessory (Bruker FRA 106) using a Nd-YAG laser (emission wavelength, 1064 nm; maximum laser power, 300 mW). The data were collected in the backscattering mode (180° excitation; resolution 4, 2 cm^{-1}) at room temperature or at 120 K in the range 4200–70 cm^{-1}. For low-temperature measurements a glass cell was used which was mounted on a sample holder fitted with an X-Y translation stage (Bruker R495). The glass cell has a vacuum shield that prevents condensation of moisture close to the measurement area and is designed to hold 5 mm NMR tubes. The sample tubes were cooled by a stream of cold nitrogen gas and the temperature at the sample was measured with a thermocouple (copper/constantan) mounted inside the glass cell. The ^{77}Se NMR samples were prepared *in situ* in thick-walled precision 10 mm NMR tubes (Wilmad Glass) fitted with J. Young O-ringette valves (ptfe stopcocks, model BST/2) in SO_2. The ^{77}Se FT-NMR spectra were recorded in the temperature range 25 to −70 °C on Varian Associates XL-200 and Unity 400 spectrometers using 10 mm broad-band probes operating at 38.164 and 76.396 MHz, respectively. For each sample, three spectra were recorded over a chemical shift range of δ −122 to 1187, 927–2230 and 1800–3200. No relaxation delays were applied. Line-broadening parameters, used in the exponential multiplication of the free induction decays, were 0–10 Hz. Further acquisition parameters were as follows (parameters for the XL-400 spectrometer in parentheses): acquisition time, 0.16 (0.10 s); pulse width, 12 (13 μs); measuring time in all cases, 30–40 min. The ^{19}F FT-NMR spectra were obtained from samples stored in thick-walled precision 5 mm NMR tubes sealed *in vacuo* and recorded in the temperature range 25 to −70 °C on a Varian Associates Unity 400 spectrometer using a 5 mm probe operating at 376.302 MHz. For each sample, two spectra were recorded over chemical shift ranges of δ −180 to 70 and −80 to 180. A relaxation delay of 4 s was applied. Line-broadening parameters, used in the exponential multiplication of the free induction decays, were 0–10 Hz. Further acquisition parameters were as follows: acquisition time, 0.6 s; pulse width, 5 μs; transmitter power, 63 dB. All samples were run unlocked and externally referenced at room temperature (r.t.) to a neat sample of Me_2Se (^{77}Se) or to a sample of $CFCl_3$ in SO_2 (^{19}F), respectively. Chemical shifts with a positive sign are correlated with shifts to high frequencies (downfield) of the reference compound. Elemental analyses were carried out by Beller Mikroanalytisches Laboratorium, Göttingen, Germany.

Sulfur dioxide (Matheson), chlorine (Air Liquid Canada) and bromine (Fisher) were vacuum distilled onto and stored over CaH_2 and P_4O_{10}, respectively. Selenium (Johnson Matthey, 1–3 mm, amorphous, ground to a powder, 99.999%), $AgSbF_6$ (Aldrich, 98%) and AsF_5 (Ozark-Mahoning) were used as received. Sulfur (precipitated; Fisher Scientific) was vacuum dried and AsF_3 (Ozark-Mahoning) was vacuum distilled onto NaF prior to use. Antimony pentafluoride (Ozark-Mahoning) was triple distilled in an all-glass apparatus and stored in a Pyrex glass vessel fitted with a Teflon valve (J. Young, UK).[23] The salts MX_3AsF_6[24a] and MX_3SbF_6[24b] (M = S or Se, X = Cl or Br) and $Se_2Br_5AsF_6$[8] were prepared as described and characterised by FT-Raman spectroscopy.

Preparations

$Se_3Cl_3AsF_6$. *From* $SeCl_3AsF_6$ *and selenium* [*equation* (1)]. The compound $SeCl_3AsF_6$ (2.629 g, 7.03 mmol) and selenium (1.111 g, 14.06 mmol) were added to one bulb of a two-bulb reaction vessel and the Teflon stem of the valve immediately replaced. The solid $SeCl_3AsF_6$ changed from white to yellow on contact with the selenium indicating that a solid-state reaction had occurred. Addition of SO_2 (7.08 g) gave a green-brown solution with no precipitate that was stirred overnight at r.t. Slow removal of the solvent over a period of 4 h into the second bulb cooled to 0 °C and filtration of the last portion (*ca.* 2 cm^3) of solution resulted in a red microcrystalline product. The total product consisted of 3.679 g (6.95 mmol) of $Se_3Cl_3AsF_6$ [FT-Raman: red microcrystalline product and red powder (from the soluble fraction) were identical]; yield 98.9% based on $SeCl_3AsF_6$ (6.87 mmol expected) [Found (Calc. for $Se_3Cl_3AsF_6$): As, 13.70 (14.15); Cl, 20.10 (20.10); F, 22.30 (21.55); Se, 44.20 (44.75%)].

Crystals suitable for single X-ray diffraction were obtained from the reaction of $SeCl_3AsF_6$ (0.466 g, 1.24 mmol) and selenium (0.197 g, 2.44 mmol) in sulfur dioxide solution (5.67 g). After stirring the green-brown solution for 6 h at room temperature, addition of sulfuryl chloride fluoride, SO_2ClF (0.8 g), and slow removal of the solvent into the second bulb (ΔT = 4 °C) produced large crystals (red and black in transmitted and reflected light, respectively). The crystals were cooled with ice–water and the solvent in the second bulb was quickly evacuated to reduce sample decomposition. The total product consisted of 0.652 g (1.23 mmol) of $Se_3Cl_3AsF_6$ (FT-Raman: red crystals and red powder identical); yield 99% based on $SeCl_3AsF_6$ and equation (1).

The identity of $Se_3Cl_3AsF_6$ was confirmed by single-crystal X-ray analysis (see below). The FT-Raman spectrum of crystalline $Se_3Cl_3AsF_6$ is shown in Fig. 6. The ^{77}Se FT-NMR spectrum of $Se_3Cl_3AsF_6$ prepared *in situ* from $SeCl_3AsF_6$ (0.919 g, 2.45 mmol) and selenium (0.393 g, 4.98 mmol) in SO_2 (3.607 g) solution, at −70 °C, gave four resonances at δ 1764 ($\nu_{\frac{1}{2}}$ = 448), 1417 (43) ($SeCl_3AsF_6$), 1345 (176) and 1159 (132 Hz) relative to neat Me_2Se (integration ratio 3.7:1:1.4:4.2); at −40 °C δ 1760 (vbr), 1367 and 1170 and at −10 °C δ 1380 and 1170 (vbr).

From selenium, chlorine and AsF_5 *in* SO_2 *solution* [*equation* (2)]. Chlorine (0.243 g, 3.42 mmol) was condensed onto selenium (0.481 g, 6.78 mmol) forming a red liquid Se_2Cl_2 containing small amounts of a yellow solid ($SeCl_4$) on warming to room temperature. Arsenic pentafluoride (0.581 g, 3.42 mmol) and SO_2 (5.5 g) were added after 1 h, the mixture stirred overnight and the volatiles removed giving a greenish black solid ($Se_3Cl_3AsF_6$: 1.158 g, 2.19 mmol; *cf.* 2.26 mmol expected; 96.8% yield based on Se). A greenish black film sublimed onto the upper walls of the reaction bulb on storage overnight leaving a reddish brown solid (0.991 g). The ^{77}Se FT-NMR spectrum (−70 °C) of the reddish brown sample dissolved in SO_2 (3.63 g) showed peaks attributable to Se_8^{2+} (δ 1969, 1525, 1073 and 1048; see ref. 25) and $Se_3Cl_3^+$ [δ 1777 ($\nu_{\frac{1}{2}}$ = 1131), 1353 (1496) and 1156 (536 Hz); integral ratio 1.4:1:1.6]. In addition, an unassigned peak at δ 1480 ($\nu_{\frac{1}{2}}$ = 133 Hz) was observed. The low-temperature FT-Raman spectrum showed vibrational bands attributable to $Se_3Cl_3AsF_6$ and an additional band at 234 cm^{-1} (unassigned).

$Se_3Cl_3SbF_6$. Dark red microcrystalline $Se_3Cl_3SbF_6$ (0.829 g, 1.43 mmol; *cf.* 1.43 mmol expected based on selenium) was quantitatively obtained from the reaction of $SeCl_3SbF_6$ (0.600 g, 1.43 mmol) and selenium (0.225 g, 2.85 mmol) in sulfur dioxide solution (6.87 g) as described for $Se_3Cl_3AsF_6$. The FT-Raman spectrum of $Se_3Cl_3SbF_6$ is shown in Fig. 6.

$S_3Cl_3AsF_6$. The compound $S_3Cl_3AsF_6$ (1.304 g, 3.33 mmol; *cf.* 3.38 mmol expected; 98.5% yield based on SCl_3AsF_6) was similarly prepared from SCl_3AsF_6 (1.106 g, 3.38 mmol) and sulfur (0.217 g, 0.85 mmol S_8) in sulfur dioxide solution (5.11 g) as described for $Se_3Cl_3AsF_6$. Red-orange microcrystalline $S_3Cl_3AsF_6$ was obtained from a clear red solution after leaving the mixture overnight with the second bulb cooled at −10 °C. Crystals suitable for single-crystal X-ray diffraction were obtained from the reaction of SCl_3AsF_6 (0.540 g, 1.65 mmol) and sulfur (0.106 g, 0.41 mmol S_8) in sulfur dioxide solution (3.99 g). After stirring the red solution for 3 h at room temperature, addition of sulfuryl chloride fluoride (1.575 g) and slow removal of the solvent into the second bulb (ΔT =

9 °C) produced large crystals that were brownish yellow and brown in transmitted and reflected light, respectively. The bulb containing the crystals was sealed and stored at −20 °C prior to mounting the crystals for X-ray diffraction. The FT-Raman spectrum of crystalline $S_3Cl_3AsF_6$ is shown in Fig. 6.

$S_3Cl_3SbF_6$. The compound $S_3Cl_3SbF_6$ (0.754 g, 1.72 mmol; *cf.* 1.81 mmol expected; 95.2% yield based on SCl_3SbF_6) was prepared from SCl_3SbF_6 (0.677 g, 1.81 mmol) and sulfur (0.134 g, 0.52 mmol S_8) in sulfur dioxide solution (5.32 g) as described for $Se_3Cl_3AsF_6$. After stirring the obtained red solution at 0 °C for 2 h, slow removal of the volatiles led to microcrystalline yellow-orange $S_3Cl_3SbF_6$. The product was characterised by its FT-Raman spectrum (see Fig. 6).

$Se_3Br_3AsF_6$ [equation (2)]. Arsenic pentafluoride (2.275 g, 13.39 mmol) and then Br_2 (2.215 g, 13.86 mmol) were condensed onto selenium (2.074 g, 26.27 mmol) in SO_2 (7.914 g). Upon warming up to room temperature a dark red-brown solution was formed in a slightly exothermic reaction. After 1 d slow removal of the solvent into the second bulb, which was cooled to 0 °C, produced dark red crystals of $Se_3Br_3AsF_6$ (5.997 g, 9.01 mmol; *cf.* expected 8.76 mmol; quantitative yield based on Se) [Found (Calc. for $Se_3Br_3AsF_6$): As, 11.25 (11.45); Br, 36.00 (36.10); F, 17.10 (16.90); Se, 35.60 (35.70%)]. The higher than expected mass may be due to some SO_2 retention. The identity of $Se_3Br_3AsF_6$ was confirmed by single-crystal X-ray analysis (see below), and the X-ray powder photograph of the bulk material was in excellent agreement with the single-crystal data. The FT-Raman spectrum of crystalline $Se_3Br_3AsF_6$ at room temperature is shown in Fig. 6. A sample of $Se_3Br_3AsF_6$ for a temperature-dependent ^{77}Se FT-NMR study was prepared *in situ* from Se (0.837 g, 10.59 mmol), AsF_5 (0.919 g, 5.41 mmol) and Br_2 (0.874 g, 5.47 mmol) in SO_2 (4.06 g). The results are shown in Fig. 5. The analagous reactions of $SeBr_3AsF_6$ and 2 Se is expected to proceed quantitatively as described in equation (1).

$Se_3Br_3SbF_6$. Dark red microcrystalline $Se_3Br_3SbF_6$ (0.734 g, 1.03 mmol; *cf.* 1.05 mmol; 98.1% based on $SeBr_3SbF_6$) was obtained from the reaction of $SeBr_3SbF_6$ (0.584 g, 1.05 mmol) and selenium (0.166 g, 2.10 mmol) in sulfur dioxide solution (4.50 g) as described for $Se_3Cl_3AsF_6$. The FT-Raman spectrum is shown in Fig. 6.

$S_3Br_3AsF_6$. The compound $S_3Br_3AsF_6$ (3.713 g, 7.07 mmol; *cf.* expected 7.09 mmol; 99.7% yield based on sulfur) was prepared as described for $Se_3Br_3AsF_6$ from sulfur (0.682 g, 2.66 mmol S_8), Br_2 (1.747 g, 10.92 mmol) and AsF_5 (1.781 g, 10.48 mmol) in SO_2 (5.12 g) [equation (2)]. Single crystals suitable for crystal structure determination were also obtained as described for $Se_3Br_3AsF_6$ [Found (Calc. for $S_3Br_3AsF_6$): As, 14.15 (14.35); Br, 45.70 (45.70); F, 21.50 (21.2); S, 18.35 (18.35%)]. Crystals of $S_3Br_3AsF_6$ are red in transmitted light and orange in the powdered form. The identity of $S_3Br_3AsF_6$ was established by single-crystal X-ray analysis (see below). The FT-Raman spectrum is shown in Fig. 6. Alternatively, $S_3Br_3AsF_6$ was prepared by the reaction of SBr_3AsF_6 and sulfur according to equation (1).

$S_3Br_3SbF_6$. The compound $S_3Br_3SbF_6$ was obtained from the reaction of SBr_3SbF_6 (2.714 g, 5.35 mmol) with sulfur (0 342 g, 1.33 mmol S_8) in SO_2 (12.5 g) solution assuming that the reaction would proceed as described by equation (1). On addition of sulfur to solid SBr_3SbF_6 an immediate change from yellow to red-orange was observed. After condensing SO_2 the reaction mixture was stirred for 18 h at room temperature giving a deep red solution over a white precipitate. Filtration and removal of the volatiles led to a red-orange solid as the soluble product ($S_3Br_3SbF_6$: 2.912 g, 5.11 mmol; *cf.* expected 5.32 mmol; 96% yield based on sulfur) and a white insoluble product ($6SbF_3 \cdot 5SbF_5$: 0.181 g; FT-Raman spectroscopy).[26] The identity of $S_3Br_3SbF_6$ was established by its FT-Raman spectrum (see Fig. 6). Attempts to obtain single crystals of $S_3Br_3SbF_6$ in SO_2 over a period of 3 d were unsuccessful, possibly due to some decomposition (SBr_3SbF_6 and S_2Br_2 identified by FT-Raman spectroscopy).

Attempts to prepare $M_2Br_3AsF_6$ (M = S or Se) by equation (2) led in both cases to mixtures of solid $M_3Br_3AsF_6$ and MBr_3AsF_6 (Raman spectrum and X-ray powder diffraction). The non-existence of the $Se_2Br_3^+$ cation in SO_2 solution was supported by ^{77}Se FT-NMR studies. The spectrum of a sample with a molar ratio of $Se:Br_2$ designed to give $Se_2Br_3^+$ showed only three resonances at δ 1735, 1288 and 1065 at −70 °C relative to neat Me_2Se (integration ratio 1:2:1) attributable to $Se_3Br_3AsF_6$ and $SeBr_3AsF_6$. Reactions designed to give $M_4Br_3AsF_6$ led to $M_3Br_3AsF_6$ as the only observed product (X-ray powder diffraction).

In the preparation of the $M_3Br_3AsF_6$ salts by equation (2) the relative molar ratio $AsF_5:Br_2$ should not differ from that as given, otherwise MBr_3AsF_6 (M = S or Se) (large excess of AsF_5) and $SeBr_4$ (large excess of Br_2) are formed as by-products (X-ray powder photograph, FT-Raman spectrum). In the preparation of $M_3X_3SbF_6$, $S_3Cl_3AsF_6$ and $Se_3Cl_3AsF_6$ (M = S or Se, X = Cl or Br) a solid-state reaction between the MCl_3AsF_6 and the chalcogen was observed. Reactants were therefore thoroughly cooled to −196 °C prior to nitrogen evacuation and addition of SO_2 to prevent loss of any possible volatile materials. Careful adherence to reaction conditions is required for the preparation of $S_3Cl_3SbF_6$ (0 °C) since previous experiments have shown that the SCl_3SbF_6 (starting material) is unstable in SO_2 solutions at room temperature (over 6 h) with respect to halogen exchange and the formation of SCl_3SbCl_6. All attempts to prepare the $S_3Cl_3SbCl_6$ compound were unsuccessful. All M_3X_3 (AsF_6/SbF_6) salts are highly soluble in SO_2, but exceeding reaction times leads to decomposition (*via* halogen exchange).

Attempted preparations

$S_3Cl_3AlCl_4$. The compound SCl_3AlCl_4 (0.472 g, 1.54 mmol) was added to sulfur (0.099 g, 0.39 mmol) in an attempt to prepare $S_3Cl_3AlCl_4$ according to equation (3). An immediate reaction in the solid state was observed and as a result a deep red liquid was formed. The liquid changed to orange over a period of 5 min. The solid-state reactions reported for other compounds of this type seem to lead to another product in this case. Another reaction on the same scale was performed, but this time the reactants were mixed in SO_2 solution, with the SCl_3AlCl_4 being washed onto the sulfur at −100 °C. The formation of a deep red solution was immediately observed. The reaction mixture was allowed to warm from −100 to −30 °C over 4 h with constant stirring. The volatiles were then removed, yielding a white material with a slightly yellow tint. The FT-Raman spectrum of the white product showed only fluorescence, which is typical of $AlCl_3$. A possible pathway for the reaction between SCl_3AlCl_4 and S_8 is given in equation (4). Since all of the products of equation (4) except the $AlCl_3$ are volatile, only $AlCl_3$ remained after pumping the product to constant weight.

$SeS_2Br_3AsF_6$ from $SeBr_3AsF_6$ and S_8 in SO_2 [equation (5)]. The compound $SeBr_3AsF_6$ (1.031 g, 2.03 mmol) and sulfur [0.140 g, 0.55 mmol; 7.5% excess according to equation (5)] were placed into the secondary bulb of a two-bulbed vessel. There was no indication of any solid-state reaction. The addition of SO_2 (4.4 g) immediately yielded a deep red solution. After stirring for 18 h at room temperature, the solution was filtered through a medium-porosity glass frit, followed by slow removal of the solvent to facilitate crystal growth. The resultant

solid contained a mixture of the starting materials, as characterised by FT-Raman spectroscopy (sulfur and $SeBr_3AsF_6$) and single-crystal X-ray diffraction [$SeBr_3AsF_6$: monoclinic, space group, $P2_1/c$; the obtained lattice constants were consistent with the data given in ref. 24(*a*)] indicating that no reaction had occurred.

$SSe_2Br_3SbF_6$ from SBr_3SbF_6 and Se in SO_2 [equation (6)]. The compound SBr_3SbF_6 (1.005 g, 1.98 mmol) followed by Se (0.312 g, 3.95 mmol) were placed into the secondary bulb of a two-bulb vessel. A small amount of an orange colour formed where the yellow SBr_3SbF_6 contacted the grey Se, indicating a solid-state reaction. The vessel was immediately evacuated, and SO_2 (4.95 g) was condensed onto the mixture, yielding a deep red solution. The reaction was allowed to stir for 3 h at 0 °C, and then filtered through a sintered-glass frit. No traces of a precipitate, Se or S_8, were visible. Removal of the volative materials led to a red solid shown by FT-Raman spectroscopy to contain $Se_3Br_3SbF_6$ and $SeBr_3SbF_6$ (attributable to less intense peaks).

Thermal stability of $M_3X_3AsF_6$ and $M_3X_3SbF_6$ salts (M = S or Se, X = Cl or Br)

The salts $M_3Br_3(AsF_6/SbF_6)$ (M = S or Se) can be stored without decomposition in a sealed glass tube under nitrogen at −20 °C over a period of at least 1 year, whereas samples of $M_3Cl_3(AsF_6/SbF_6)$ (M = S or Se) stored under the same conditions started to decompose after 4 months indicated by the formation of an orange-red (possibly Se_2Cl_2) or yellow (possibly S_2Cl_2) liquid film on the surface of the crystal as well as loss of crystallinity.

Crystallography

Crystals were examined in a dry-box using a Wild M3 microscope of long focal length mounted outside the dry-box. A number of crystals were flame sealed in rigorously dried capillary tubes. The data for $S_3Br_3AsF_6$, $Se_3Cl_3AsF_6$ and $Se_3Br_3AsF_6$ were collected at room temperature on an Enraf-Nonius CAD-4 automated diffractometer operating in the ω–2θ scan mode with graphite-monochromated Mo-Kα radiation. Diffraction intensities for $S_3Cl_3AsF_6$ were measured on a Rigaku AFC5R diffractometer with graphite-monochromated Mo-Kα radiation at a temperature of −60 ± 1 °C using ω–2θ scans. Details of the data collections are given in Table 1.

The structures were refined by full-matrix least squares with all atoms assigned anisotropic thermal parameters, except for the structure of $Se_3Br_3AsF_6$ where only the selenium and bromine atoms were assigned anisotropic displacement parameters. The data for the four crystal structures were corrected for Lorentz and polarisation effects. In addition, the structural data (except for $Se_3Cl_3AsF_6$) were corrected for absorption using the program DIFABS[27b] ($S_3Br_3AsF_6$ and $Se_3Br_3AsF_6$) and ψ scan corrections ($S_3Cl_3AsF_6$).[27a] Calculations were performed using the personal computer implementation of the NRCVAX program package[28] and the programs SHELXS 86[29] and SHELX 76[30] (for $S_3Cl_3AsF_6$), respectively. Scattering factors were taken from ref. 31 and effects of anomalous dispersion were included in F_c using the values of Cromer.[32]

The structure of $Cl_2SSSCl(AsF_6)$ contains disordered $S_3Cl_3^+$ cations. There was some indication that the two disordered atoms were at slightly different sites. Attempts to separate the atoms between their two sites were unsuccessful. As a compromise the bridging atoms in the two disordered rings were refined as sulfur in one ring (cation 1) and as chlorine (cation 2) in the other. The $S_3Br_3^+$ cations in $S_3Br_3AsF_6$ are also disordered. The bridging atoms, labelled as S/Br, were refined as 50% S and 50% Br. There is only one crystallographically independent disordered AsF_6^- anion. All fluorine atoms were refined having 50% occupancy. The structure of $Se_3Br_3AsF_6$ consists of two crystallographically different $Se_3Br_3^+$ cations, one of which was refined as an ordered $BrSe^+$-(Br)SeSeBr cation and the other as disordered with the bridging atoms, labelled as Se/Br, having occupancies 50% Se, 50% Br. The two crystallographically different AsF_6^- anions have distorted-octahedral symmetry.

Complete atom coordinates, thermal parameters, and bond lengths and angles have been deposited at the Cambridge Crystallographic Data Centre. See Instructions for Authors, *J. Chem. Soc., Dalton Trans.*, 1996, Issue 1.

Molecular orbital calculations

The RHF/STO-3G* calculations were performed on $S_3H_3^+$, $S_3Cl_3^+$ and $Se_3Cl_3^+$ using the GAUSSIAN 92 suite of programs, *i.e.* the highest *ab initio* level available for selenium using GAUSSIAN 92.[20] The starting geometries for $S_3H_3^+$ and $S_3Cl_3^+$ were both based on the observed crystal structure of $Se_3Cl_3^+$, using the bond orders from $Se_3Cl_3^+$ to estimate the appropriate S–Cl, S–H, S–S bond distances. The bond angles for $S_3H_3^+$ and $S_3Cl_3^+$ were determined by keeping all bond lengths and the dihedral angle X(2)–M(1)–M(2)–M(3) constant, and allowing all other angles to geometry optimise. The effect on the total energy of the system of allowing the X(2) atom to move out of the X(2)–(M1)–M(2)–M(3) plane (M = S or Se, X = H or Cl) and of altering the chalcogen–chalcogen bond alternation was investigated to study the influence of the observed intracationic contact and chalcogen–chalcogen bond alternation. The molecular orbitals of the cations were generated by extended-Hückel calculations using the corresponding STO-3G* geometry parameters and the program CACAO.[19] A complete listing of all data is given in SUP 57126.

Discussion

Preparation of $M_3X_3AsF_6$ and $M_3X_3SbF_6$ (M = S or Se, X = Cl or Br)

The reaction of stoichiometric quantities of chalcogen (S, Se) with bromine and AsF_5 in SO_2 led to essentially quantitative formation of $M_3Br_3AsF_6$ [equation (2)]. The analogous

$$MX_3AF_6 + 2M \xrightarrow{SO_2(l)} M_3X_3AF_6 \quad (1)$$

(M = S or Se, X = Cl or Br, A = As or Sb)

$$6M + 3X_2 + 3AsF_5 \xrightarrow{SO_2(l)} 2M_3X_3AsF_6 + AsF_3 \quad (2)$$

(M = S or Se, X = Cl or Br)

reaction designed to give $Se_3Cl_3AsF_6$ led to a mixture of $Se_3Cl_3AsF_6$, $Se_8(AsF_6)_2$ and an unidentified species (^{77}Se FT-NMR spectra). However, we have succeeded in preparing the compounds $M_3Cl_3AsF_6$ essentially quantitatively by the reaction of MCl_3AsF_6 and the corresponding chalcogen M (Se or S) using SO_2 as solvent [equation (1)]. A similar reaction of SCl_3SbF_6 and $\frac{1}{4}S_8$ led quantitatively to $S_3Cl_3SbF_6$. However, the reaction of SBr_3SbF_6 and sulfur led to less than 100% of $S_3Br_3SbF_6$ and small amounts of a complex Sb^V, Sb^{III}, F-containing species ($6SbF_3{\cdot}5SbF_5$)[26] implying some reduction of Sb^V (SbF_6^-) to Sb^{III} (SbF_3). The reduced antimony fluoride was insoluble in the solvent SO_2 and therefore easily separated from the very soluble $S_3Br_3SbF_6$. The volatile products contained SOF_2, SO_2F_2 and SO_2BrF (^{19}F FT-NMR spectra) indicating an oxidative fluorination of the solvent had taken place accounting for the observed reduced antimony fluoride.

Attempts to prepare $S_3Cl_3AlCl_4$ by the reaction of SCl_3AlCl_4 and $\frac{1}{4}S_8$ [equation (3)] were unsuccessful, leading instead to decomposition products, possibly described by equation (4).

$$SCl_3AlCl_4 + \tfrac{1}{4}S_8 \xrightarrow{SO_2(l)} S_3Cl_3AlCl_4 \quad (3)$$

$$SCl_3AlCl_4\ (s) + \tfrac{1}{4}S_8\ (s) \longrightarrow S_2Cl_2\ (l,\ yellow) + SCl_2\ (l,\ red) + AlCl_3\ (s,\ white) \quad (4)$$

The compounds $M_3X_3AsF_6$ (M = S or Se, X = Cl or Br) were characterised in the solid state by single-crystal X-ray diffraction. The bulk samples of $Se_3Cl_3AsF_6$ and $M_3Br_3AsF_6$ (M = S or Se) gave good elemental analyses and X-ray powder diffraction photographs that correlated with the single-crystal data. The FT-Raman spectra of all $M_3X_3AsF_6$ and $M_3X_3SbF_6$ salts showed the presence of $M_3X_3^+$ and $(As/Sb)F_6^-$ anions. For comparison the FT-Raman spectrum of $Se_2Br_5AsF_6$ was measured and assigned.

Attempts to prepare $M_2X_3^+$ led to a mixture of MX_3^+ and $M_3X_3^+$ and attempts to prepare $M_4X_3^+$ led to $M_3X_3^+$ and an unidentified product. The reaction of MX_3^+ (M = S or Se, X = Cl or Br) with the corresponding chalcogen (S, Se) is a formal insertion into the M–X bond of the MX_3^+ cation, to our knowledge only known for neutral species (*cf.* formation of S_xCl_2 from sulfur and S_2Cl_2). The first steps (i) and (ii) in the SCl_3^+ reaction with S_8 are envisaged as shown in Scheme 1. The number of M–X and M–M bonds is identical in the products and reactants for equation (1). The driving force is likely positive charge delocalisation and intracationic contacts (see below).

Attempts to synthesise the mixed-chalcogen cations $(Br_2SeSSBr)^+$ and $(Br_2SeSSeBr)^+$ according to equations (5) and (6)

$$SeBr_3AsF_6 + \tfrac{1}{4}S_8 \xrightarrow{SO_2(l)} Br_2SeSSBrAsF_6 \quad (5)$$

$$SBr_3SbF_6 + 2Se \xrightarrow{SO_2(l)} Br_2SeSSeBrSbF_6 \quad (6)$$

were unsuccessful, but SBr_3SbF_6 and selenium possibly reacted as shown in equation (7).* Assuming that these mixed chalcogen cations would adopt similar structures to those of the known $M_3X_3^+$ cations (M = S or Se, X = Cl or Br), the energetics of these and similar reactions leading to the possible cations $(Br_2SeSSBr)^+$, $(Br_2SSeSeBr)^+$ and $(Br_2SeSSeBr)^+$ were investigated, based on bond and atomic ionisation energies and ignoring lattice energies and entropy changes. The results of these estimates implied that the formation of $(Br_2SeSSBr)$ according to equation (5) is thermodynamically unfavourable by *ca.* 70 kJ mol^{-1} in agreement with the observed results.† The cation $(Br_2SeSSeBr)^+$ was determined to be the most energetically favoured structure of the possible combinations, and found to be energetically favoured over the starting materials. However, attempts to prepare this species led to a mixture of $Se_3Br_3^+$ and $SeBr_3^+$ as characterised by FT-Raman spectroscopy and estimated to be allowed (−10 kJ mol^{-1}), but in fact not as energetically favoured as (6) (−87 kJ mol^{-1}). Similar calculations were carried out for the chlorine cations with similar results.†

$$2SBr_3SbF_6 + 4Se \xrightarrow{SO_2(l)} Se_3Br_3SbF_6 + SeBr_3SbF_6 + \tfrac{1}{4}S_8 \quad (7)$$

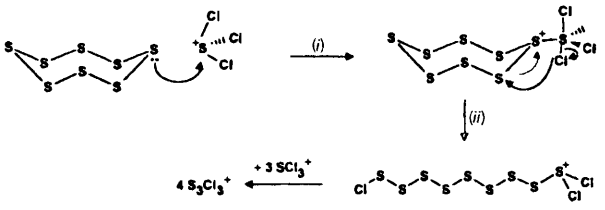

Scheme 1

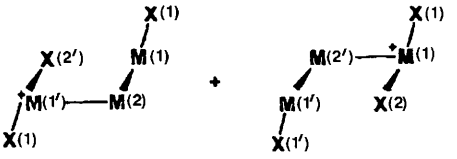

1 **2**

(M = S, X = Cl or Br; M = Se, X = Br)

The salts $M_3X_3AF_6$ (M = S or Se, X = Cl or Br, A = As or Sb) contain the first examples of $M_3X_3^+$ cations, which are formally the salts of the non-existent neutral species S_3X_4 (X = Cl or Br) and Se_3X_4 (*cf.* F_3SSSF). The cations Se_9Cl^+,[14] S_7Br^+,[6] $Se_2Br_5^+$[7] and $M_3X_3^+$ (M = S or Se, X = Cl or Br) are, as far as we are aware, the only examples of fully characterised lower chalcogen/halogen cations.

Crystal structures of the $M_3X_3AsF_6$ (M = S or Se, X = Cl or Br) salts

The crystal structures of the $M_3X_3AsF_6$ (M = S or Se, X = Cl or Br) salts consist of sheets containing $M_3X_3^+$ cations (bond distances are given in Fig. 1, angles are listed in Tables 2 and 3) and AsF_6^- anions with cation–anion as well as cation–cation interactions. The crystal packing is given in Figs. 2 and 3. The $Se_3Cl_3AsF_6$ salt contains all ordered $Se_3Cl_3^+$ cations, $Se_3Br_3AsF_6$ contains both ordered and disordered $Se_3Br_3^+$ cations, whereas the $S_3Cl_3^+$ and $S_3Br_3^+$ cations in $S_3Cl_3AsF_6$ and $S_3Br_3AsF_6$ are all disordered (see Fig. 1). The structure of $S_3Cl_3AsF_6$ shows two crystallographically distinct cations arranged about different symmetry centres, both cations are disordered. The disorder in the cations can be reasonably accounted for by the superimposition of two ordered cations, *e.g.* **1** and **2**, each with a structure similar to that of the ordered $(X_2SeSeSeX)^+$ cation (X = Cl or Br). Thus, the bond distances and angles in the disordered $Se_3Br_3^+$ cation are roughly an average of the corresponding values in the ordered $Se_3Br_3^+$ cation.‡ The observed bond distances and angles in $S_3X_3^+$ (X = Cl or Br) correspond to the superimposition of those expected for the sulfur analogues of **1** and **2**. For example, the out-of-plane S–Br distance in the disordered $S_3Br_3^+$ cation is 2.150(6) Å, approximately a 1 : 1 average of the S^{IV}–Br [S–Br in SBr_3^+ 2.142(8); S^{II}–Br in S_2Br_2, 2.24 Å (2.19 Å, estimated from the Schomaker–Stevenson equation)§] and represents good evidence for the presence of the $S_3X_3^+$ cations. The disorder in the $S_3X_3AsF_6$ (X = Cl or Br) structures precludes

* Elemental sulfur was not detected by FT-Raman spectroscopy of the product, possibly because it was amorphous.

† The estimated values for the enthalpies of reaction, ΔH/kJ mol^{-1}, were as follows: equation (5), −71 for $(Br_2SeSSBr)^+$ and (with Cl instead of Br) 43 for $(Cl_2SeSSCl)^+$; equation (6), −87 for $(Br_2SeSSeBr)^+$ and (with Cl instead of Br) −3 for $(Cl_2SeSSeCl)^+$; for reaction (7), −16. The values for the bond energies (kJ mol^{-1}) of S–S (266), Se–Se (192), S–Cl (271), S–Br (218) and Se–Cl (251) and for the ionisation potentials (kJ mol^{-1}) for S (1000) and Se (941) were taken from ref. 33(*a*) and those for the atomisation energies (kJ mol^{-1}) for Se (218) and S (279) from ref. 33(*b*). The S–Br bond energy (226 kJ mol^{-1}) was given in ref. 34 and the Se–S bond energy estimated to be half the sum of the S–S and Se–Se bond energies. The theoretical calculations indicated that the energy change involved in the reaction –SS– + –SeSe– ⟶ 2 –SeS– is small (0 to −2 kJ mol^{-1}),[33c] and the reaction of gaseous diatomic molecules $S_2(g) + Se_2(g) \longrightarrow 2\ SeS(g)$ is only slightly endothermic (ΔH = 5.4 ± 2.9 kJ mol^{-1}).[33d] Changes in lattice solvation energies have been ignored.

‡ Observed and estimated bond distances (Å) in the disordered $Se_3Br_3^+$ cation: *d*[Se(4)–Se/Br] 2.206(7) (obs.), 2.230 (estimated); *d*[Se(4′)–Se/Br] 2.943(7) (obs.), 2.997 (estimated). Bond distances were estimated by the equations $d[Se(4)\text{–}Se/Br] = \frac{1}{2}\{d[Se(1)\text{–}Br(2)] + d[Se(2)\text{–}Se(3)]\}$ and $d[Se(4')\text{–}Se/Br] = \frac{1}{2}\{d[Se(1)\text{–}Se(2)] + d[Se(3)\cdots Br(2)]\}$.

§ Schomaker–Stevenson distance for S–Br = $r_{S,cov} + r_{Br,cov} - 0.09|\chi_S - \chi_{Br}|$ Å,[37] where $r_{S,cov}$ = 1.04 Å, $r_{Br,cov}$ = 1.11 Å, χ_S = 2.6, χ_{Br} = 3.0; χ_S, χ_{Br} electronegativities according to Pauling.[38]

detailed discussions of the geometry of the cations. However, the similarity in the geometries of the disordered $S_3X_3^+$ and the ordered $Se_3X_3^+$ cations is further supported by comparison of their FT-Raman spectra (see below). The extent of the disorder may relate to the strength of the M···F cation–anion interactions that are proportional to the sum of the M···F bond valence units (v.u.s) and decrease in the order $Se_3Cl_3^+$ (0.65) > $Se_3Br_3^+$ (0.62) > $S_3Cl_3^+$ (0.35) > $S_3Br_3^+$ (0.31 v.u.) [*e.g.* M···F contacts in MX_3AsF_6 salts, $SeCl_3^+$ (0.45) ≈ $SeBr_3^+$ (0.46) > SCl_3^+ (0.28) > SBr_3^+ (0.17 v.u.)].*

The $Se_3Cl_3^+$ cations in $Se_3Cl_3AsF_6$ are joined into strands parallel to the *a* axis *via* four Se···Cl contacts [Se(3)···Cl(3h) 3.497(6) (twice), Se(1)···Cl(1a) 3.783(6), Se(2)···Cl(3e) 3.785(6) Å], the latter only slightly greater than the sum of the isotropic van der Waals radii[36] of selenium and chlorine (3.65 Å) (see Fig. 3).† The strands are joined into sheets of $(Se_3Cl_3^+)_x$ parallel to the *ac* plane by two Se(2)···Cl(3) [Se(2)···Cl(3c), Cl(3)···Se(2k)] intercationic contacts at 3.678(6) Å. These Se···Cl contacts are significant, or the cation would be expected to be completely surrounded by contacts to the anion. They are likely to arise from electrostatic attraction between the partially positively charged selenium and negatively charged chlorine atoms. The arrangement of the cations into sheets is similar in the structures of $S_3X_3AsF_6$ (X = Cl or Br) with similar cation–cation contacts (see Fig. 2). The latter structures are not discussed in detail due to the cation disorder.

The average As–F bond distances and F–As–F angles in $S_3X_3AsF_6$ (X = Cl or Br; see SUP 57126) and $Se_3Br_3AsF_6$ (Table 3) are 1.68 Å and 90°. The average As–F distances in the AsF_6^- anions of the $M_3X_3AsF_6$ salts are slightly shorter than those in $KAsF_6$ [1.719(3) Å, 90.0(2)°][41] likely reflecting greater cation–anion contacts in the potassium salt. There is a significant deviation in the As–F bond distances from those of the ideal octahedral geometry of the AsF_6^- anions in $Se_3Cl_3AsF_6$ (Table 2) and this can be in part related to the strengths of the contacts made by a particular fluorine atom to the selenium atoms. The sums of the fluorine contact bond valencies (v.u.s) and As–F bond lengths (Å) (in decreasing order) are: F(2), 0.271, 1.698(13); F(4), 0.145, 1.682(13); F(1), 0.066, 1.618(15); F(3), 0.076, 1.617(16); F(5), 0.00, 1.608(18) and F(6), 0.161, 1.594(17). So that overall the stronger the contacts, the longer are the As–F bonds.

Cation–anion contacts to the $Se_3Cl_3^+$ and the ordered $Se_3Br_3^+$ cation are listed in Tables 2 and 3 and the corresponding Figures have been deposited. The bond distances in the $S_3X_3^+$ cations are given in Fig. 1 and angles are listed in Tables 2 and 3. Additional bond distances and angles in $M_3X_3AsF_6$ have been deposited.

Structure and bonding in the ordered $Se_3Cl_3^+$ and $Se_3Br_3^+$ cations. The ordered $Se_3X_3^+$ (X = Cl or Br) cations (see Fig. 1) have C_1 symmetry and contain a triselenium chain. The X(2)···Se(1)Se(2)Se(3) atoms are essentially coplanar [torsion angles: 1.2(1), $Se_3Cl_3^+$; −2.9(3)°, $Se_3Br_3^+$] and the intracationic Se(3)···X(2) contacts are significantly less than the sum of the corresponding van der Waals radii[36] (3.65 and 3.75 Å for Cl and Br) of selenium and the halogen [3.289(5), $Se_3Cl_3^+$; 3.436(7) Å, $Se_3Br_3^+$]. These contacts are 10 and 8% less, respectively, than the sum of the isotropic van der Waals radii of selenium and the related halogen and reflect attractions (weakly bonding) between the atoms Se(3) and X(2). The $Se(1)^+$ (three-co-ordinate)–Se(2) (two-co-ordinate) bonds [2.551(3) ($Se_3Cl_3^+$); 2.558(6) Å ($Se_3Br_3^+$)] are considerably longer than the Se(2) (two-co-ordinate)–Se(3) (two-co-ordinate) [2.191(3) ($Se_3Cl_3^+$); 2.207(6) Å ($Se_3Br_3^+$)] bonds implying the presence of substantial, partial, $4p_\pi$–$4p_\pi$ bonding between the atoms Se(2) and Se(3) (bond orders > 1, see Table 4). As far as we are aware, the Se(2)–Se(3) bonds are the shortest selenium–selenium bond lengths known for an isolated compound, and the bond alternation is the greatest so far observed in selenium chains or rings (see Table 4). They represent more examples of exceptions to the 'double bond rule', that is the thermodynamic

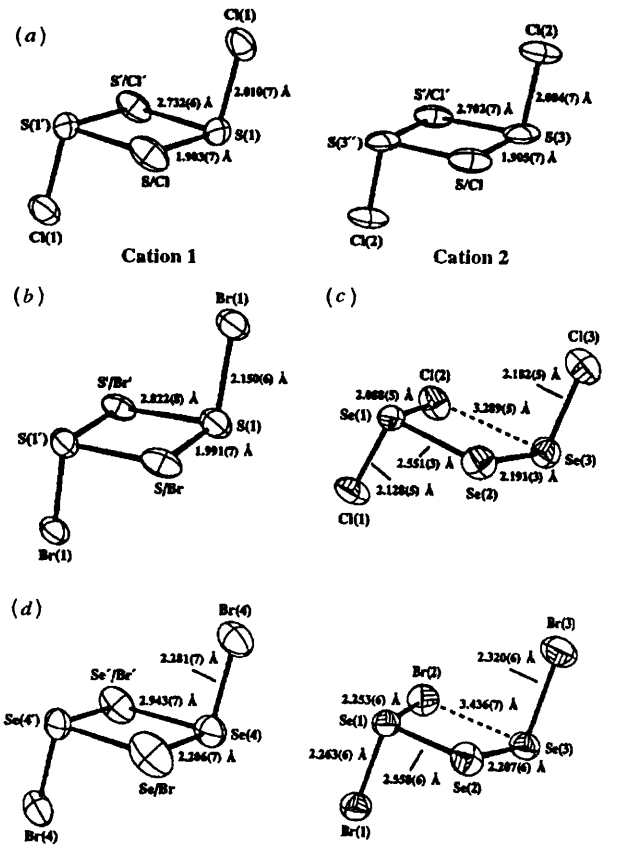

Fig. 1 Structures of the $M_3X_3^+$ cations: (*a*) $S_3Cl_3^+$ [two crystallographically different disordered cations; the bridging atoms S(2), S(2′) (cation 1) and Cl(3), Cl(3′) (cation 2) are labelled as S/Cl and S′/Cl′ for consistency with the other disordered structures]; (*b*) $S_3Br_3^+$ (disordered; S/Br, disordered position with S:Br = 50%:50% occupancy); (*c*) $Se_3Cl_3^+$ (bond distances corrected for libration {the anisotropic displacement parameters (a.d.p.s) for the cation were fitted using TLS[35] rigid-body motion analysis; weighted $R = [\Sigma w(U_o - U_c)/w(U_o^2)]^{\frac{1}{2}}$ for all U was 0.061, where $U_{hkl} = F_{hkl}/F_{000}$}:[35] Se(1)–Se(2) 2.569, Se(2)–Se(3) 2.208, Se(1)–Cl(1) 2.144, Se(1)–Cl(2) 2.107 and Se(3)–Cl(3) 2.182 Å; (*d*) $Se_3Br_3^+$ [ordered and disordered (Se/Br: disordered position with Se:Br = 50%:50% occupancy)]. Dihedral angles X(2)···M(3)–M(2)–M(1) are cation 2: S′/Cl′–S(3′)–S/Cl–S(3) 0.0(3), cation 1: Cl(1′)–S(1′)–S(2)–S(1) 0.0(3), S′/Br′–S(1)–S/Br–S(1′) 0.00(20), Cl(2)···Se(3)–Se(2)–Se(1) 1.2, Br(2)···Se(3)–Se(2)–Se(1) −2.9(3), Se′/Br′–Se(4′)–Se/Br–Se(4) 0.0(4)° (see also SUP 57126). The thermal ellipsoids are scaled to enclose 50% of the probability density (ORTEP, included in the NRCVAX program package)[28]

* It has been shown that the strength of the $S^{IV}\cdots F$ and $Se^{IV}\cdots F$ contacts can be assessed by the relative magnitude of the bond valences (*S*) in valency units (v.u.s) and is directly correlated to the positive charge on the chalcogen. An increase in positive charge on an atom leads to an increase in the bond valence sum around the atom and is accompanied by the formation of additional bonds and contacts (interionic and/or intracationic) equal to the charge on the atom. The bond valence *S* in valence units (v.u.s) is given by $S = (R/R_0)^{-N}$, where *R* is the observed bond distance (Å), R_0 = 1.73 Å and N = 4 for $Se^{IV}\cdots F$ and R_0 = 1.55 Å and N = 3.8 for $S^{IV}\cdots F$ (see ref. 39). It was assumed that all S and Se atoms have a valency of 4 which is clearly not the case and therefore the values we quote are only approximate.

† It is possible that the contacts, which are slightly greater than the sum of isotropic van der Waals radii, are in fact less than the sum of the corresponding anisotropic van der Waals radii (see ref. 40) and therefore reflect weak but significant intercationic interactions. In addition, the interactions may be weakly electrostatic in origin and still be of significance even if greater than the sum of the van der Waals radii.

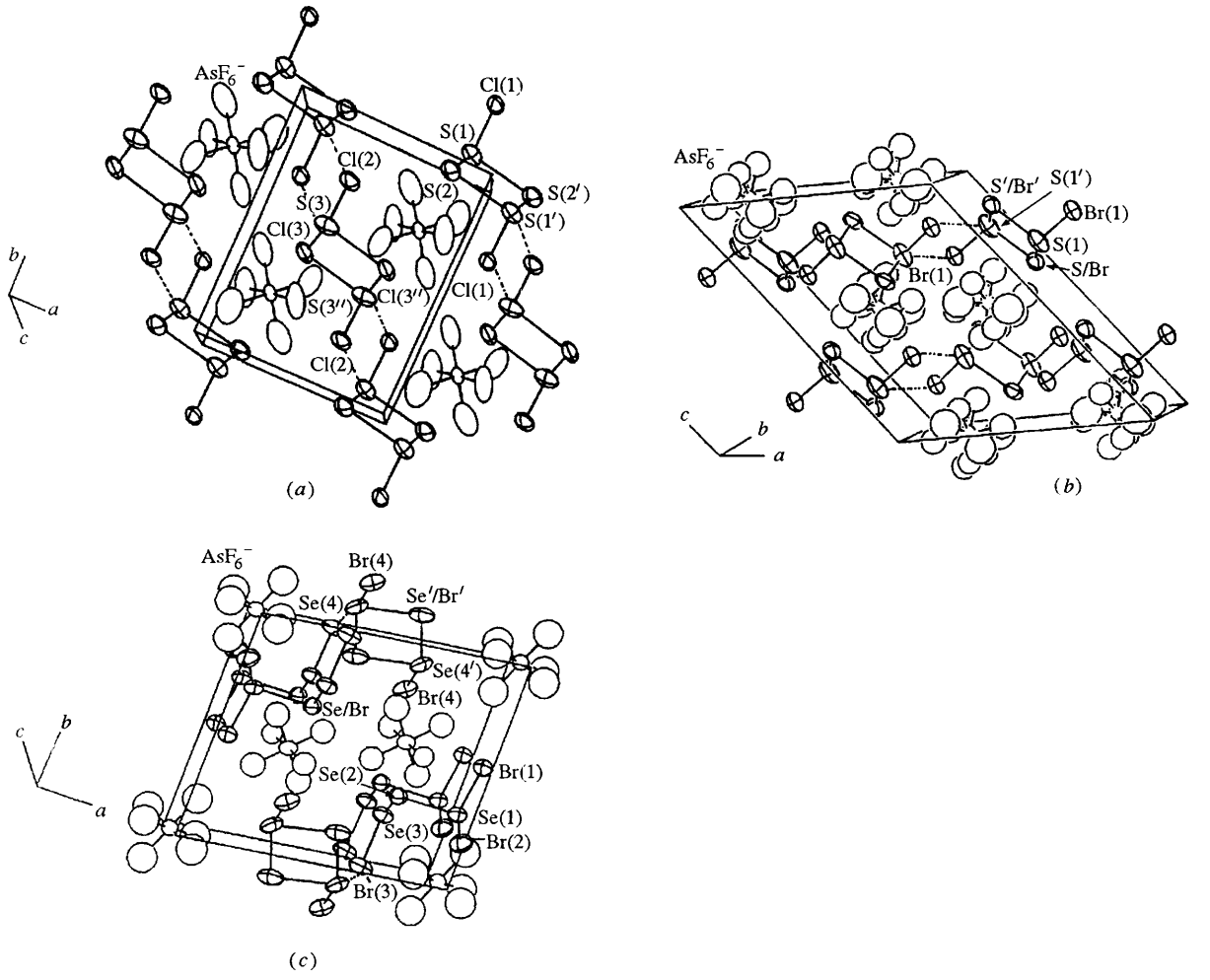

Fig. 2 Crystal packing in (*a*) $S_3Cl_3AsF_6$, (*b*) $S_3Br_3AsF_6$ and (*c*) $Se_3Br_3AsF_6$, showing some cation–cation contacts: – – –, S(1) · · · Cl(2) 3.586(6); – · – · –, S(3) · · · Cl(1) 3.656(9); – · · –, S(1) · · · Br(1)/S(1′) · · · Br(1) 3.696(6) and · · ·, Br(3) · · · Se(4) 3.560(7) Å [includes contacts that are less than the sum of the van der Waals radii for S · · · Cl (≤ 3.55 Å) and S · · · Br (≤3.65 Å)]

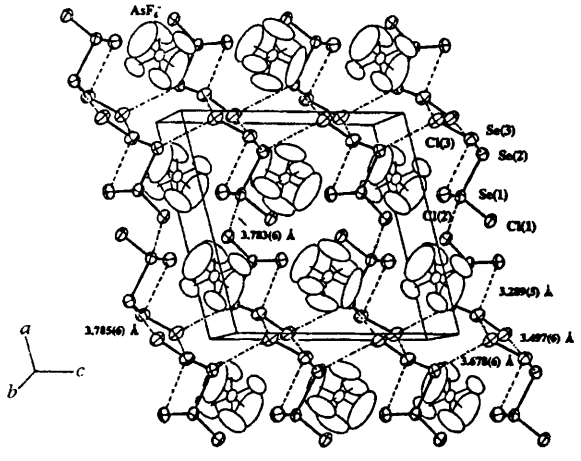

Fig. 3 Crystal packing in $Se_3Cl_3AsF_6$ showing intracationic and cation–cation contacts: – – –, Se(3) · · · Cl(3) (intracationic contact); – · · –, Se(3) · · · Cl(3h); – ·· – ·· –, Se(1) · · · Cl(1a); – – · – –, Se(2) · · · Cl(3e); – · – · –, Se(2) · · · Cl(3c) and Cl(3) · · · Se(2k)

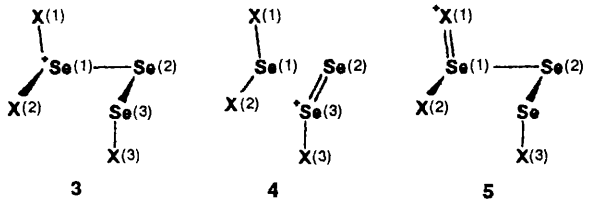

preference for homopolyatomic σ bonds over np_π–np_π bonds for heavier main-group elements ($n > 3$).[44] In valence-bond terms the bond alternation and positive-charge delocalisation from Se(1) to Se(3) [but not Se(2)] can be accounted for by the valence-bond structure **3** as well as **4** making a significant contribution to the bonding within the cations. This is reflected also in the calculated charges on the selenium atoms in $Se_3Cl_3^+$ obtained from *ab initio* calculations, *i.e.* charges on Se(1) > Se(2) [Se(1), +0.56; Se(2), +0.19; Se(3), +0.27; see also below]. The calculated Se(1)–Se(2) and Se(2)–Se(3) bond orders ($Se_3Cl_3^+$, 0.44, 1.73; $Se_3Br_3^+$, 0.4, 1.6)* imply that the contributions of **3** and **4** are about equal and that the shorter Se(2)–Se(3) bond contains significant π-bond character. This view is further supported by the similar total bond orders around Se(1) and Se(3) [$Se_3Cl_3^+$: 2.81, 2.69; $Se_3Br_3^+$: 2.76, 2.60] (see Table 5). These are less than in SeX_3^+ (X = Cl, 3.68; X = Br, 3.43) but greater than around Se(2) ($Se_3Cl_3^+$, 2.17;

* Bond orders were estimated using a variation of Pauling's bond distance–bond order relationship, $D(n') = D_1 - b \log n'$, where n' is the bond order, $D(n')$ the observed bond length, D_1 the single-bond distance and b a constant.[38] Selenium–selenium bond orders were estimated using the relationship $D(n') = 2.336 - 0.611 \log n'$, where 2.336(6) Å is the observed single Se–Se bond distance in Se_8.[42] The constant 0.611 was determined by assuming that the bond order in Se_2(g) [bond distance = 2.152(3) Å] is 2.[43] Sulfur–sulfur bond orders were estimated using the relationship $D(n') = 2.048 - 0.526 \log n'$ given in ref. 12(*b*) using for the variable D_1 the value for the S–S single bond distance observed in S_8 (2.048 Å). Bond lengths and orders for $Se_3Cl_3^+$: Se(1)–Se(2) 2.551, 0.4; Se(2)–Se(3) 2.191, 1.7; Se(1)–Cl(1) 2.128, 1.1; Se(1)–Cl(2) 2.088, 1.3; Se(3)–Cl(3) 2.182 Å, 0.9.

Table 1 Crystal parameters and intensity data measurements for $M_3X_3AsF_6$ (M = S or Se; X = Cl or Br)

	Compound			
Parameter	$S_3Cl_3AsF_6$	$S_3Br_3AsF_6$	$Se_3Cl_3AsF_6$	$Se_3Br_3AsF_6$
Formula	$AsCl_3F_6S_3$	$AsBr_3F_6S_3$	$AsCl_3F_6Se_3$	$AsBr_3F_6Se_3$
M	391.45	524.8	532.15	665.5
Crystal dimensions/mm	0.23 × 0.25 × 0.20	0.30 × 0.30 × 0.40	0.36 × 0.24 × 0.16	0.44 × 0.44 × 0.44
T/K	213	295	295	295
Crystal system	Triclinic	Monoclinic	Monoclinic	Triclinic
Space group	$P\bar{1}$	$C2/c$	$P2_1/c$	$P\bar{1}$
a/Å	8.026(5)	15.094(1)	12.162(1)	8.0353(6)
b/Å	10.023(5)	7.8141(8)	7.8457(9)	10.0716(8)
c/Å	7.609(5)	11.926(1)	12.108(1)	11.442(1)
α/°	111.70(4)			79.595(8)
β/°	115.87(5)	127.528(8)	105.052(7)	87.379(8)
γ/°	82.36(5)			76.773(6)
U/Å^3	511.7(6)	1115.5(2)	1115.7(2)	885.8(1)
Z (molecules per cell)	2	4	4	3
D_c/Mg m^{-3}	2.547	3.07	3.187	3.74
$F(000)$	372	961	961	880
λ(Mo)/Å[a]	0.710 69 (K$\bar{\alpha}$)	0.7093 (Kα1)	0.710 69 (K$\bar{\alpha}$)	0.7093 (Kα1)
μ(Mo-Kα)/mm^{-1}	4.64	14.26	13.49	22.12
Range ($2\theta_{max}$)	46	50	50	45
No. unique reflections	1226	969	1945	2303
No. observed reflections	929 [$I_o > 3\sigma(I_o)$]	565 [$I_o > 2.5\sigma(I_o)$]	1458 [$I_o > 0.5\sigma(I_o)$]	1191 [$I_o > 2.5\sigma(I_o)$]
No. variables	118	52	134	134
$R = \Sigma(\|F_o\| - \|F_c\|)/\Sigma(\|F_o\|)$	0.059	0.073	0.083	0.069
$R' = [\Sigma w(\|F_o\| - \|F_c\|)^2/\Sigma(wF_o)^2]^{\frac{1}{2}}$	0.059	0.084	0.084	0.075
Goodness of fit[b]	2.35	2.53	1.65	2.09
Largest shift/error in final least squares cycle	0.517	0.014	0.001	0.026

[a] The Nonius software generates the data on Mo-Kα1 radiation and makes adjustments for Mo-Kα2 radiation. The software for the Rigaku diffractometer works with the average value for Mo-K$\bar{\alpha}$. [b] $[\Sigma w(|F_o| - |F_c|)^2/(n_d - n_p)]^{\frac{1}{2}}$, where n_d = number of data (reflections) and n_p = number of parameters. Data refined on F, $w = 1$.

$Se_3Br_3^+$, 2.0; see Table 5).* On the other hand, the average Se(1)$^+$–X distances [X = Cl, 2.108(5); Br, 2.258(8) Å] are similar to those in SeX_3^+ (see Table 6) which are the shortest bonds of their class so far reported in isolated compounds. They are significantly shorter (and stronger) than the two-co-ordinate Se(3)–X bonds [Se(3)–Cl, 2.182(5); Se(3)–Br, 2.320(6) Å] which are both similar to related neutral two-co-ordinate Se–X bond lengths (see Table 6). The bond orders for the Se(1)$^+$–X bonds are calculated to be greater than one [X = Cl, 1.18; Br, 1.18 (averages)]. The increase of the bond order Se$^+$–X may be due in part to $3p_\pi \longrightarrow 4d_\pi$ (Cl–Se$^+$)/$4p_\pi \longrightarrow 4d_\pi$ (Br–Se$^+$) back bonding, accompanied by positive-charge delocalisation onto the halogen atom indicating that the resonance structure **5** and, others that are similar, is significant. Consistently, the F···X (X = Cl or Br) contacts to the X atoms of the M(1)X_2^+ unit are stronger than to the halogen atom of the M(3)–X(3) fragment. Interestingly, an intercationic contact Cl(3)···Se(3) [3.497(6) Å] is formed instead of a Cl(3)···F contact in $Se_3Cl_3AsF_6$. The sum of the Se(1)···F bond valencies [$Cl_2Se(1)^+SeSeCl$, 0.316; $Br_2Se(1)^+SeSeBr$, 0.263 v.u.] is significantly greater than the sum of the bond valencies for the corresponding Se(3)···F interactions [Cl_2-$Se^+SeSe(3)Cl$, 0.161; $Br_2Se^+SeSe(3)Br$, 0.172 v.u.] which is nearly equal to those for the formally neutral Se(2) atom ($Se_3Cl_3^+$, 0.176; $Se_3Br_3^+$, 0.186 v.u.) (see Table 5). Both $Se_3X_3^+$ cations have a significant intrahalogen X(2)···Se(3) contact [$Se_3Cl_3^+$, 3.289(5); $Se_3Br_3^+$, 3.436(7) Å] that may have neutralised some of the (δ+) charge on the two-co-ordinate Se(3) atom by delocalisation of electron density to Se(3). Consistently, the bond angles Se(1)–X(2)···Se(3) of 84.26(16) ($Se_3Cl_3AsF_6$) and 79.64(19)° ($Se_3Br_3AsF_6$) imply that the halogen is acting as an electron donor. Similar situations have been observed in S_7I^+, $Se_6I_2^{2+}$ and S_7Br^+.[1,5,6] In addition, both Se(1)–X(2) distances [Se(1)–Cl(2) 2.088(5), Se(1)–Br(2) 2.253(6) Å] within the intracationic ring are shorter than the out-of-plane Se(1)–X(1) distances [Se(1)–Cl(1) 2.128(5), Se(1)–Br(2) 2.263(6) Å] consistent with loss of electron density from an antibonding orbital of Se(1)$^+$–X(2) by donation to Se(3).† This will lead to a reduction of π*-electron density in the Se(1)$^+$–X(2) bond, a decrease in its bond length and an increase in positive charge on the atom X(2).

The stability and structures of a number of polychalcogen–halogen cations[1a,5,18,49] have been attributed in part to maximisation of charge delocalisation, maximisation of bond-length alternation [leading to np_π–np_π bonding ($n > 3$)] and intramolecular chalcogen–halogen contacts (leading to cluster-like structures and serving to delocalise positive charge). As a consequence all known structures of polyatomic chalcogen–halogen cations maximise chalcogen–chalcogen bond alternation. Consistently, all attempts to prepare the cations $(X_2SeSeX)^+$ and $(X_2SeSeSeSeX)^+$ led to mixtures containing SeX_3^+ and $(X_2SeSeSeX)^+$, implying a high stability for the alternating selenium–selenium bond arrangement.

The $XSe^+(X)SeSeX$ cation is structurally very similar to the $Se_2Se^+SeSeCl$ fragment in $Se_7^+SeSeCl$,[14] with the halogen atoms replacing the cyclic two-co-ordinate selenium atoms adjacent to Se$^+$ as illustrated in Fig. 4. The $(X_2MMMX)^+$ cation is indeed the simplest $M_nX_y^{q+}$ species (M = S or Se; X = univalent atom group; n, y and q are integers) in which bond alternation along a chain or ring of M atoms can occur, originating from the three-co-ordinate M^+ atom. Interestingly, attempts to prepare $I_2SeSeSeIAsF_6$ led to $Se_6I_2(AsF_6)_2$.[5] In fact, no $M_nI_y^{q+}$ cation containing an M^{II}–I bond has so far been characterised, consistent with the non-existence of stable neutral non-sterically hindered sulfur and selenium iodides.[1a]

* We anticipated for two-co-ordinate selenium to form two bonds, and for three-co-ordinate positively charged selenium three, or up to four bonds if there is delocalisation of charge from the halogen.

† However, if the Se(3) atom is two-co-ordinate and neutral [which it is not, as its total valence is significantly higher than that of the two-co-ordinate Se(2); see Table 5] then the electrons in the p orbital perpendicular to the SeSeX plane are pointing directly towards X(2).

Table 2 Bond angles (°) and anionic bond distances (Å) for $S_3Cl_3AsF_6$ and anionic bond distances, interionic contacts[a] (Å) and selected angles for $Se_3Cl_3AsF_6$ with estimated standard deviations (e.s.d.s) in parentheses[b]

$S_3Cl_3AsF_6$			
Cation 1[c]		Cation 2[c]	
S(2')[S'/Cl']–S(1')–S(2)[S/Cl]	87.4(3)	Cl(3'')[S'/Cl']–S(3'')–Cl(3)[S/Cl]	88.0(3)
S(1')–S(2)–S(1)	92.6(3)	S(3'')–Cl(3)[S/Cl]–S(3)	92.0(3)
Cl(1)–S(1)–S(2')[S'/Cl']	96.3(2)	Cl(2)–S(3)–Cl(3'')[S'/Cl']	97.3(3)
Cl(1)–S(1)–S(2)[S/Cl]	106.3(3)	Cl(2)–S(3)–Cl(3)[S/Cl]	106.3(3)
AsF_6^-			
As(1)–F(1)	1.67(2)	As(1)–F(4)	1.68(2)
As(1)–F(2)	1.67(2)	As(1)–F(5)	1.727(14)
As(1)–F(3)	1.67(2)	As(1)–F(6)	1.66(2)
$Se_3Cl_3AsF_6$			
Se(1) · · · F(2d)	2.688(13)	Se(2) · · · Cl(3c)	3.678(6)
Se(1) · · · F(4b)	2.804(14)	Se(3) · · · Cl(3h)	3.497(6)
Se(1) · · · F(1c)	3.414(14)	Cl(3) · · · Se(2k)	3.678(6)
Se(2) · · · F(2d)	3.078(14)	Cl(1) · · · F(2d)	3.229(18)
Se(2) · · · F(3d)	3.294(15)	Cl(1) · · · F(5j)	3.044(23)
Se(1) · · · Cl(1a)	3.783(6)	Cl(2) · · · F(5l)	3.053(22)
Se(2) · · · Cl(3e)	3.785(6)	Cl(3) · · · F(4b)	3.622(19)
Cl(2)–Se(1)–Se(2)	96.84(16)	Cl(3)–Se(3)–Se(2)	104.41(18)
Se(2)–Se(1)–Cl(1)	99.97(15)	Cl(2) · · · Se(3)–Se(2)	76.02(11)
Cl(2)–Se(1)–Cl(1)	99.77(22)	Se(3) · · · Cl(2)–Se(1)	84.26(16)
Se(3)–Se(2)–Se(1)	102.87(9)		
Cl(1)–Se(1)–Se(2)–Se(3)	102.4(2)	Cl(2)–Se(1)–Se(2)–Se(3)	1.2(1)
Se(1)–Se(2)–Se(3)–Cl(3)	87.0(2)		
Se(2)–Se(3)–F(6g)	91.2(6)	Cl(1)–Se(2)–F(2d)	57.3(3)
Se(2)–Se(3)–Cl(3h)	150.86(13)	Cl(1)–Se(2)–F(3d)	91.7(3)
Cl(1)–Se(1)–F(2d)	83.3(5)	Cl(3)–Se(3)–Cl(3h)	96.16(18)
Cl(1)–Se(1)–F(4b)	174.2(5)	Se(2)–Se(1)–F(4b)	174.2(5)
Se(2)–Se(1)–F(2d)	83.3(5)	Cl(3)–Se(3)–F(6g)	164.3(6)
AsF_6^-			
As(1)–F(1)	1.618(15)	As(1)–F(4)	1.682(13)
As(1)–F(2)	1.698(13)	As(1)–F(5)	1.608(18)
As(1)–F(3)	1.617(16)	As(1)–F(6)	1.594(17)

[a] Includes all contacts less or slightly greater than the sum of the isotropic van der Waals radii for Se,F 3.37; Se,Cl 3.65; and Cl,F 3.22 Å.[36] [b] Symmetry relations: a $1-x, \frac{1}{2}+y, \frac{1}{2}-z$; b $1-x, \frac{1}{2}+y, \frac{3}{2}-z$; c $x, \frac{3}{2}-y, -\frac{1}{2}+z$; d $1-x, 2-y, 1-z$; e $-x, \frac{1}{2}+y, \frac{1}{2}-z$; g $1-x, 1-y, 1-z$; h $-x, -\frac{1}{2}+y, \frac{1}{2}-z$; j $x, y, -1+z$; k $1-x, \frac{1}{2}+y, \frac{3}{2}-z$; l $x, \frac{3}{2}+y, \frac{1}{2}+z$. The bond distances for the $S_3Cl_3^+$ and $Se_3Cl_3^+$ cations are given in Fig. 1. Bond angles for the anions have been deposited. [c] The bridging atoms S(2), S(2') (cation 1) and Cl(3), Cl(3'') (cation 2) are labelled as S/Cl and S'/Cl' in Fig. 1 for consistency with the other disordered structures.

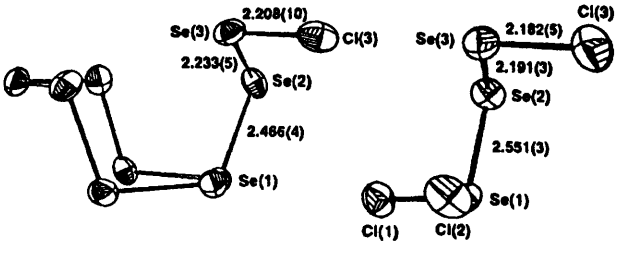

Fig. 4 Comparison between the $Se_3Cl_3^+$ and Se_9Cl^+ cations (bond distances in Å)

Characterisation of the cation $Se_3X_3^+$ (X = Cl or Br) in SO_2 solution by ^{77}Se FT-NMR spectroscopy

The $Se_3X_3^+$ cation (X = Cl or Br) is expected to give three resonances in the integration ratio 1 : 1 : 1. The ^{77}Se FT-NMR spectrum of $Se_3Br_3AsF_6$ prepared *in situ* in SO_2 solution at −70 °C consistently showed three resonances of about equal intensity (see Fig. 5). This is consistent with the $Se_3Br_3^+$ cation retaining its solid-state structure in solution or that of the rotamer predicted to be more stable in the gas phase (see below). At −45 °C the two peaks at δ 1263 and 1065 have collapsed into a broad peak at δ 1184 consistent with an intercationic exchange process rendering Se(1) and Se(3) equivalent, as shown in equation (8).

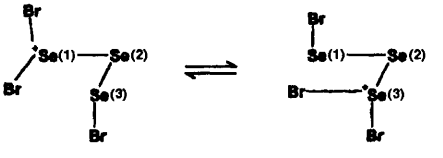

(8)

The ^{77}Se NMR chemical shifts of the three-co-ordinate, positively charged selenium atoms in $Se_6I_2^{2+}$ and $Se_4I_4^{2+}$ are much lower than those of the two-co-ordinate selenium atoms, consistent with the high chemical shift of Se(2) and the low chemical shifts of Se(1) and Se(3) (see Table 7).[50] Therefore, the peak at δ 1263 is assigned to Se(1) and that at δ 1065 to Se(3). The resonance at δ 1735 corresponds to the central selenium atom Se(2), the highest chemical shift reported for a selenium–bromine species (see Table 7). The ^{77}Se FT-NMR spectrum obtained for the $Se_3Cl_3^+$ cation is not inconsistent with the presence of this cation in solution, although the three resonances at δ 1777, 1353 and 1156 are not of equal intensity, possibly due to an intermolecular exchange process.

Table 3 Bond angles (°) for $S_3Br_3AsF_6$ and anionic bond distances (Å) for $Se_3Br_3AsF_6$, interionic contacts[a] and selected angles for the ordered $Se_3Br_3^+$ cation with e.s.d.s in parentheses[b]

$S_3Br_3AsF_6$			
S′/Br′–S(1′)–S/Br	92.60(25)	S(1)–S′/Br′–S(1′)	87.4(3)
Br(1)–S(1)–S′/Br′	97.1(3)	Br(1)–S(1)–S/Br	107.4(3)
$Se_3Br_3AsF_6$			
$Se_3Br_3^+$ (disordered)			
Se′/Br′–Se(4′)–Br(4)	88.24(22)	Br(4)–Se(4)–Se′/Br′	93.96(23)
Se(4)–Se/Br–Se(4′)	91.76(23)	Br(4)–Se(4)–Se/Br	104.1(3)
$Se_3Br_3^+$ (ordered)			
Se(1) · · · F(4c)	2.79(3)	Se(3) · · · F(5e)	3.24(3)
Se(1) · · · F(7d)	2.97(4)	Br(2) · · · F(9f)	3.39(4)
Se(2) · · · F(2c)	3.22(3)	Br(1) · · · F(8c)	3.05(4)
Se(2) · · · F(4c)	3.05(3)	Br(3) · · · F(3f)	3.34(3)
Se(3) · · · F(1e)	3.149(25)	Br(3) · · · Se(4f)	3.560(7)
Br(2)–Se(1)–Se(2)	98.97(22)	Br(3)–Se(3)–Se(2)	105.15(24)
Se(2)–Se(1)–Br(1)	99.30(21)	Br(2) · · · Se(3)–Se(2)	77.58(18)
Br(2)–Se(1)–Br(1)	102.59(25)	Se(3) · · · Br(2)–Se(1)	79.64(19)
Se(3)–Se(2)–Se(1)	103.73(22)		
Br(1)–Se(1)–Se(2)–Se(3)	101.6(6)	Br(2)–Se(1)–Se(2)–Se(3)	91.1(5)
Se(1)–Se(2)–Se(3)–Br(3)	−2.9(3)		
Se(2)–Se(3)–F(1e)	83.5(5)	F(1e)–Br(1)–F(4c)	106.1(6)
Se(2)–Se(3)–F(5e)	112.1(5)	F(1e)–Br(1)–F(8c)	108.4(8)
Br(1)–Se(1)–F(4c)	91.0(7)	Br(2)–Br(3)–F(3f)	140.0(5)
Br(1)–Se(1)–F(7d)	166.2(8)	Br(1)–Se(2)–F(2c)	72.9(5)
Se(2)–Se(1)–F(4c)	69.3(6)	Br(1)–Se(2)–F(4c)	64.4(6)
Br(3)–Se(3)–F(1e)	165.7(5)	F(1e)–Se(3)–F(5e)	44.0(7)
Br(3)–Se(3)–F(5e)	136.7(5)		
AsF_6^-			
As(1)–F(7)	1.68(4)	As(2)–F(3)	1.69(3)
As(1)–F(8)	1.68(4)	As(2)–F(4)	1.73(3)
As(1)–F(9)	1.66(4)	As(2)–F(5)	1.63(3)
As(2)–F(1)	1.683(25)	As(2)–F(6)	1.65(3)
As(2)–F(2)	1.73(3)		

[a] Includes all contacts less than the sum of the isotropic van der Waals radii for Se,F 3.37; Se,Br 3.75; and Br,F 3.35 Å.[36]. [b] Symmetry equivalents: c $1-x, 1-y, 1-z$; d $1-x, -y, 1-z$; e $2-x, 1-y, 1-z$; f $2-x, -y, 1-z$. Bond angles for the anions have been deposited.

Table 4 Selenium–selenium bond distances in various chalcogen–halogen cations containing a three-co-ordinate selenium atom in comparison with the bond distances in Se_2(gas) and Se_8

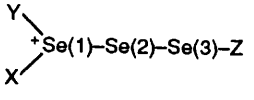

	Distance[a]/Å		Bond order[b]			
Compound	*d*[Se(1)–Se(2)]	*d*[Se(2)–Se(3)]	Se(1)–Se(2)	Se(2)–Se(3)	Δ[c]/Å	Ref.
$(Se_6I)_n \cdot nAsF_6$	2.365(3)	2.292(4)	0.9	1.2	0.07	5
$Se_7SeSeCl(SbCl_6)$	2.367(4)[d]	2.309(5)[d]	0.9	1.1	0.06	14
	2.430(4)[d]	2.270(4)[d]	0.7	1.3	0.16	
	2.466(4)[e]	2.233(5)[e]	0.6	1.5	0.23	
$Se_6I_2(AsF_6)_2$	2.475(2)[f]	2.227(2)	0.6	1.5	0.25	5
$Br_2SeSeSeBr(AsF_6)$	2.558(6)	2.207(6)	0.4	1.6	0.35	This work
$Cl_2SeSeSeCl(AsF_6)$	2.551(3)	2.191(2)	0.4	1.7	0.36	This work
Se_2(g)		2.152(3)		2.0		43
Se_8		2.336(6)		1.0		42

[a] X, Y = –Se–, Cl, or Br; Z = –Se–, Cl, Br or I. The distances are not corrected for libration (see Fig. 1 for the corrected values for $Cl_2Se^+SeSeCl$). [b] Calculated according to footnote * on p. 2559. [c] Bond alternation, $d(Se_A–Se_B) - d(Se_B–Se_C)$. [d] Bond distances within the seven-membered ring. [e] Bond distances in the exocyclic >Se–Se–Se–Cl fragment. [f] Average of Se(three-co-ordinate)–Se(two-co-ordinate) bond distances.

FT-Raman spectra of $M_3X_3(As/Sb)F_6$ salts (M = S or Se, X = Cl or Br)

The FT-Raman spectra for the $M_3X_3(As/Sb)F_6$ salts are shown in Fig. 6 and the measured vibrational frequencies and their assignments are listed in Table 8. The spectra show vibrations attributable to the AF_6^- anions (A = As or Sb) and $M_3X_3^+$ cations (M = S or Se, X = Cl or Br). For the $(X_2MMMX)^+$ ions with approximately C_1 symmetry 12 fundamental vibrations are expected which are both IR and Raman active: five stretching, five bending modes and two torsions.[54] The irreducible representation[55] for the vibrations of the $(X_2MMMX)^+$

Table 5 Sum of the bond orders[a] at the selenium atoms and bond valency units[b] for the Se · · · F contacts in $Se_3Cl_3^+$ and $Se_3Br_3^+$ in comparison with $SeCl_3^+$ and $SeBr_3^+$[c]

Atom	$SeCl_3^+$	$Se_3Cl_3^+$	$Se_3Br_3^+$	$SeBr_3^+$
Se(1) Σ b.o. (Σ v.u.)	3.68 (0.450)	2.81 (0.316)	2.76 (0.263)	3.43 (0.458)
Se(2) Σ b.o. (Σ v.u.)		2.17 (0.176)	2.0 (0.186)	
Se(3) Σ b.o. (Σ v.u.)		2.69 (0.161)	2.60 (0.172)	
Total Σ v.u. of the Se · · · F contacts	0.45	0.65	0.62	0.46

[a] The bond orders for the Se–Se bonds were calculated according to footnote * on p. 2559, those for Se–Cl and Se–Br were calculated using Pauling's equation $D(n') = D_1 - b \log n'$ with D_1(Se–Cl) = 2.16, D_1(Se–Br) = 2.31 Å (see ref. 38). [b] Bond valencies were obtained using the equation given in footnote * on p. 2558. [c] Observed in $SeCl_3AsF_6$[24b] and $SeBr_3SbF_6$.[24a]

Table 6 Observed Se–X (X = Cl or Br) bond distances[a] and Se–X/X–Se–X vibrational bands for selenium–chlorine and –bromine compounds

Compound	Average Se–X/Å	Bands/cm^{-1}	Ref.
$SeCl_3AsF_6$	2.096(2)	437 (ν_{asym}), 418 (ν_{sym}), 207 (δ_{sym}), 156 (δ_{asym})	24(*b*)
$Cl_2SeSeSeCl(AsF_6)$	2.108(5) (Cl_2Se)	440 (ν_{asym}), 418 (ν_{sym}), 189 (δ_{sym}), 151 (δ_{asym})	This work
	2.182(5) (SeCl)	365 (ν)	
$SeCl_2$ (g)	2.157(3)	415 (ν), 377 (ν), 153 (δ)	13
$SeCl_4$	2.170(5)	392 (ν_{asym}), 358 (ν_{sym})	13
O=$SeCl_2$ (g, 100 °C)	2.204(5)	362 (ν_{asym}), 390 (ν_{sym}), 167 (δ)	13
Se_2Cl_2	2.204(1)	358 (ν_{asym}), 358 (ν_{sym}), 148 (δ_{asym}), 133 (δ_{sym})	13
$SeOCl_3$	2.234(eq.)	318 (ν_{eq})	13
	2.452(ax.)	249 (ν_{ax}), 229 (ν_{ax})	
$(SeCl_2)_2N(AsF_6)$	2.155(4)	282 (ν_{asym}), 330 (ν_{sym}), 207 (δ), 176 (δ)	45
Cs_2SeCl_6	2.41	280 [$\nu(a_{1g})$], 242 [$\nu(e_u)$], 275 [$\nu(f_{1u})$]	13
SeO_2Cl^-	2.453(1)	193 (ν)	13
$Br_2SeBrSeBr_2(AsF_6)$	2.279(6) (Br_2Se)	301 (ν_{asym}), 294 (ν_{sym}), 119 (δ_{sym})	7, This work
$SeBr_3SbF_6$	2.269(8)	303/298 (ν_{asym}), 291 (ν_{sym}), 138 (δ_s)	24(*a*), 46
$Br_2SeSeSeBr(AsF_6)$	2.258(6) (Br_2Se)	323 (ν_{asym}), 297 (ν_{sym}), 141 (δ_{sym})	This work
	2.320(6) (SeBr)	275 (ν)	
β-$SeBr_4$	2.37	267 (ν_{asym}), 248 (ν_{asym}), 228 (ν_{sym}), 141 (δ_{sym}),	13, 47
Se_2Br_2	2.366(1)β	254 (ν_{asym}/ν_{sym})	13
	2.357(1)α		
$SeBr_2$	2.32(2)	290 (ν_{asym}), 266 (ν_{sym}), 105 (δ) (in MeCN)	13, 47
$SeBr_2$(tmtu)[b]	2.594(3)	184 (ν_{asym}), 159 (ν_{sym}), 112 (δ)	48
$OSeBr_2$	2.358(2)	297 (ν_{sym}), 270 (ν_{asym}), 102 (δ)	13

[a] Bridging Se–X–Se bond distances and frequencies have not been included. [b] tmtu = Tetramethylthiourea.

Table 7 Selenium-77 FT-NMR chemical shifts (δ) of selenium–halogen cations relative to Me_2Se

Compound	Three-co-ordinate (positively charged) Se	Neutral two-co-ordinate Se (–Se–*Se*–Se–)	Two-co-ordinate Se (–Se–*Se*–X, X = Cl or Br)
$Se_6I_2^{2+}$[a]	483.5	1312.5	
$Se_4I_4^{2+}$[a]	979.3	1554.3	
$SeCl_3^+$[b]	1419.6		
$SeBr_3^+$[c]	1326.1		
SeI_3^+[a]	835.7		
$[Br_2SeBrSeBr_2]^+$[c]	1331.1		
$[Br_2Se(1)Se(2)Se(3)Br]^+$[d]	1263 [Se(1)]	1735 [Se(2)]	1065 [Se(3)]
$[Cl_2Se(1)Se(2)Se(3)Cl]^+$[d]	1353 [Se(1)]	1777 [Se(2)]	1156 [Se(3)]

[a] Measured at −80 °C.[18,50] [b] At −40 °C, this work. [c] At 20 °C.[7] [d] At −70 °C, this work.

ion is as in equation (9), where A is the symmetry type and

$$\Sigma_{vib} = 12\ A\ (IR, Raman, pol) \quad (9)$$

pol means polarised. Consistently, the FT-Raman spectra show peaks attributable to the stretching vibrations of the strong and weak M–M bonds in the $M_3X_3^+$ cations (M = S or Se, X = Cl or Br), M^+X_2 stretches (similar to those in MX_3AsF_6 and MX_3SbF_6; see Tables 6, 9) and to another M–X stretch at lower frequency corresponding to the vibration of the neutral M–X bond (similar to MX_2 and M_2X_2; see Tables 6, 9). The spectra provide further evidence for the similarities of the structures of the ordered and disordered $M_3X_3^+$ cations (see Table 8).

Although it is not possible to obtain the exact bond distances for the $S_3X_3^+$ cations from the structure determination due to the disorder, the sulfur–sulfur and –halogen distances can be estimated from the observed stretching frequencies in the FT-Raman spectra of the $S_3X_3AsF_6$ salts. Average values for sulfur–sulfur stretching frequencies, found for several related sulfur compounds, are compared with the appropriate average sulfur–sulfur bond length in Table 10. From these data the linear relationship (10) was derived (correlation coefficient,

$$\nu(SS)/cm^{-1} = 3060.55 - 1263.14\ d(S\text{–}S)/Å \quad (10)$$

$r = -0.97$). This is shown graphically in Fig. 7, which demonstrates the linearity in the trend of the S–S stretching-frequency term with the bond length in neutral and ionic sulfur species containing heteroatoms (*cf.* O, halogen). Only sulfur compounds containing ordinary σ-S–S or (σ + π)-S–S bonds were considered; (π*–π*)-S–S bonds [*cf.* S_4N_4, $(S_3N_2^+)_2$] were excluded (see ref. 49 for a detailed discussion of π*–π* bonds). Similar linear relationships were established for diatomic

Table 8 FT-Raman bands (cm^{-1}) of $M_3X_3AF_6$ (A = As or Sb, M = Se or S, X = Cl or Br) with relative intensities in parentheses (for atom labelling see ordered $Se_3Cl_3^+$, $Se_3Br_3^+$ in Fig. 1 and structure **7** below)

$S_3Cl_3AsF_6$	$S_3Cl_3SbF_6$	$S_3Br_3AsF_6$	$S_3Cl_3SbF_6$	$Se_3Cl_3AsF_6$	$Se_3Cl_3SbF_6$	$Se_3Br_3AsF_6$	$Se_3Br_3SbF_6$	Assignments[a]
		689(3)				696(2)	660(2)	$\nu(As/SbF_6^-)$, $\nu_3(F_{1u})^b$
679(10)	647(24)	674(17)	644(21)	682(20)	648(49)	678(10)	644(16), 640(7)	$\nu(As/SbF_6^-)$, $\nu_1(A_{1g})^b$
614(7, br)	603(10)	605(5)	599(7)					ν[S(2)–S(3)][c]
577(1)	569(6)	566(3)	562(3)	584(2)	581(4), 557(2)	576(1), 565(2)	575(2), 555(3)	$\nu(As/SbF_6^-)$, $\nu_2(E_g)^b$
556(6, br)	556(9)	447(10)	443(13)	440(30)	435(27)	323(8)	313(36)	ν[X(2)–M(1)][d]
522(4, br)	521(7)	405(6)	402(12)	418(6)	412(12)	297(15)	299(7), 293(7)	ν[X(1)–M(1)][d]
468(7, br)	477(9)	375(13)	379(13)	365(20)	367(24)	278(14)	283(30)	ν[M(3)–X(3)][e]
		394(5)		398(6), 389(6)				$\nu(AsF_6^-)$, $\nu_4(F_{1u})^b$
368(3)	281(24)	367(8)	279(10)	376(6)		372(5), 367(5)	272(12)	$\nu(As/SbF_6^-)$, $\nu_5(F_{2g})^b$
				323(15)	319(17)	310(15)	313(36)	ν[Se(2)–Se(3)][c]
275(10)		247(28)	246(34)	189(20)	187(57)	142(32)	145(46)	δ[M(1)–M(2)–M(3)]
223(100)	234(100)	227(100)	228(100)	170(100)	174(100)	162(100)	165(100)	ν[M(1)–M(2)]
	216(24)				165(27)			
256(30)	258(50)	204(81)	204(60)	151(30)	152(48)	124(25)	124(23)	δ[X(3)–M(3)–M(2)]
170(2)	175(2)	144(15)	143(24)	124(10)	130(14)	110(42)	109(30)	δ[X(2)–M(1)–M(2)], δ[X_2M(1)]
135(70)	139(73)	136(14)	136(21)	109(30)	109(49)	94(4)		δ[X(1)–M(1)–M(2)], δ[X_2M(1)], torsion $S_3Cl_3^+$
		98(45)	96(39)	93(5)		84(16)	81(15)	Torsion $M_3X_3^+$

[a] The tentative assignments given were based on comparison between band positions, relative intensities, and bond distances observed for related species (see Tables 6, 9, 10). In addition, HF/6-31G* vibrational frequency calculations on $S_3Cl_3^+$ (geometry **II**, see Fig. 8) support these tentative assignments, although some mixing was observed. [b] By comparison with AsF_6^- ($CsAsF_6$) and SbF_6^- ($LiSbF_6$) salts.[51] [c] Also supported by the fact that the intensities of the sulfur–sulfur stretching bands increase with increasing S–S bond distance[52] and we have found this is also the case for selenium.[53] [d] The observed $Se(1)^+X_2$ stretching frequencies are comparable to those for the SeX_3^+ cations (see Table 6). The Se(3)–X(3) stretching frequencies are observed at 278 ($Se_3Br_3AsF_6$) and 365 cm^{-1} ($Se_3Cl_3AsF_6$), respectively are equal to the average of the Se–X stretching frequencies found for SeX_2; see Table 6. [e] The assignments for the S–X stretching vibrations in the $S_3X_3(As/Sb)F_6$ salts (X = Cl or Br) were made by comparison with S–X stretching frequencies of related compounds (see Table 9).

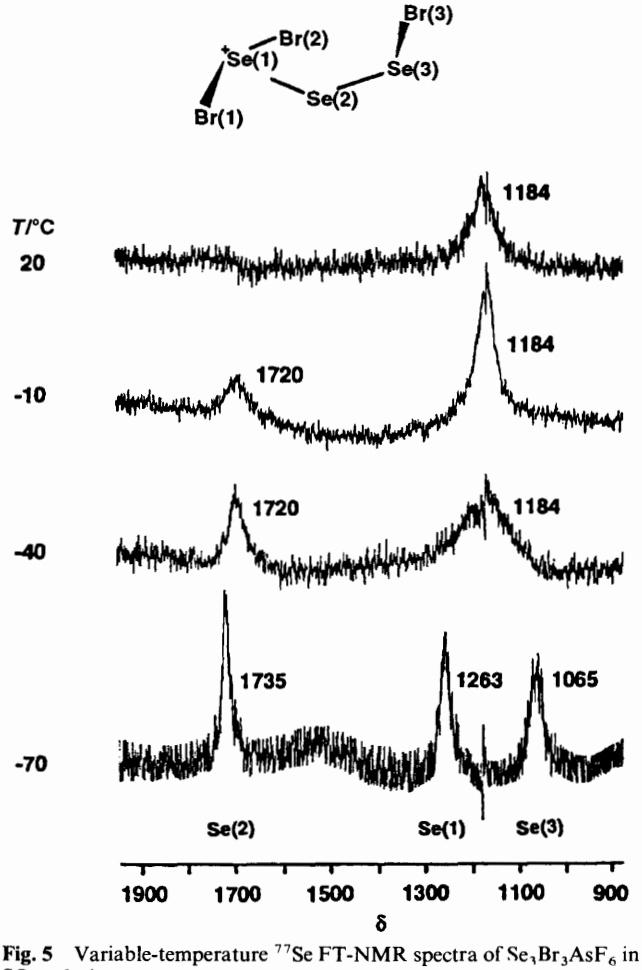

Fig. 5 Variable-temperature ^{77}Se FT-NMR spectra of $Se_3Br_3AsF_6$ in SO_2 solution

sulfur–sulfur molecules or ions and for sulfur-ring systems (S_n, n = 6, 8 or 12) and S_8O in ref. 69. The S(2)–S(3) and S(1)–S(2) bond distances in $S_3Br_3^+$ ($S_3Cl_3^+$) can be estimated from the S–S stretching frequencies at 605 (614) and 227 (223) cm^{-1} to be 1.944 (1.937) Å and 2.243 (2.246) Å, respectively. The corresponding bond orders are 1.6 (1.6) and 0.4 (0.4). Equations (11) and (12) were derived from stretching

$$\nu(\text{S–Br})/cm^{-1} = 1432.16 - 468.68\, d(\text{S–Br})/Å \quad (r\ -0.88) \quad (11)$$

$$\nu(\text{S–Cl})/cm^{-1} = 1913.90 - 696.54\, d(\text{S–Cl})/Å \quad (r\ -0.90) \quad (12)$$

frequencies and bond distances in related sulfur–bromine/chlorine compounds (see Table 9 and Fig. 7). The $X_2S(1)^+$ (X = Cl or Br) bond distances (d_{av}) are estimated from the SX stretching frequencies at 447/405 cm^{-1} [$Br_2S(1)$] and 550/522 cm^{-1} [$Cl_2S(1)$] (for labelling of the atoms see Fig. 8) to be 2.15 ($S_3Br_3^+$) and 1.97 Å ($S_3Cl_3^+$) using equations (11) and (12). The S(3)–X(3) bond distances are estimated as 2.25 ($S_3Br_3^+$) and 2.07 Å ($S_3Cl_3^+$) from the S(3)–X(3) stretching frequencies at 375 ($S_3Br_3^+$) and 468 cm^{-1} ($S_3Cl_3^+$).

In addition, the bond distances in the $S_3X_3^+$ cations (X = Cl or Br) were extrapolated from the corresponding bond distances in $Se_3X_3^+$ (see Fig. 1) and the single-bond distances of S–S (2.048 Å in S_8),[70] Se–Se (2.336 Å in Se_8),[42] S^+–X (d_{av} in SX_3AsF_6), Se^+–X [d_{av} in $SeX_3(As/Sb)F_6$][4], and the bond distances for covalent S–X and Se–X single bonds.* The

* Estimates of the bond distances in the $S_3X_3^+$ cations can also be made by extrapolation of the Se–Se [2.554(6), 2.211(6) Å], Se^+–X and Se–X bond distances in $Se_3X_3^+$ (X = Cl, Br; see Fig. 1) and the single-bond distances of S–S (2.048 Å in S_8),[70] Se–Se (2.336 Å in Se_8),[42] S^+–X [d_{av}; 2.145 (SBr_3AsF_6),[4] 1.970 Å (SCl_3AsF_6)[12a]], Se^+–X [d_{av}; 2.27 ($SeBr_3SbF_6$),[4] 2.096 Å ($SeCl_3AsF_6$)[24b]], S–X [d_{cov}; 2.18 (S–Br), 2.03 Å (S–Cl)][38] and Se–X [d_{cov}; 2.31 (Se–Br), 2.16 Å (Se–Cl)][38] according to the following equations: $d_{SS}(S_3X_3^+)/Å = [d_{SS}(S_8)/d_{SeSe}(Se_8)]d_{SeSe}(Se_3X_3^+)$; $d_{S^+X}(S_3X_3^+)/Å = [d_{S^+X}(SX_3^+)/d_{Se^+X}(SeX_3^+)]d_{av,Se^+X}(Se_3X_3^+)$; $d_{SX}(S_3X_3^+)/Å = [d_{cov}(S–X)/d_{cov}(Se–X)]d_{SeX}(Se_3X_3^+)$. Estimates of bond angles in the $S_3X_3^+$ cations: $S^+X_2(S_3X_3^+)/° = [\angle S^+X_{2,av}(SX_3^+)/\angle Se^+X_{2,av}(SeX_3^+)] \times \angle Se^+X(Se_3X_3^+)$, ∠ 102.3 (X = Cl), 105.5° (X = Br); $\angle SSX(S_3X_3^+)/° = [\angle SSX(S_2X_2)/\angle SeSeX(Se_2X_2)] \times \angle SeSeX(Se_3X_3^+)$, 109 (X = Cl), 103° (X = Br).

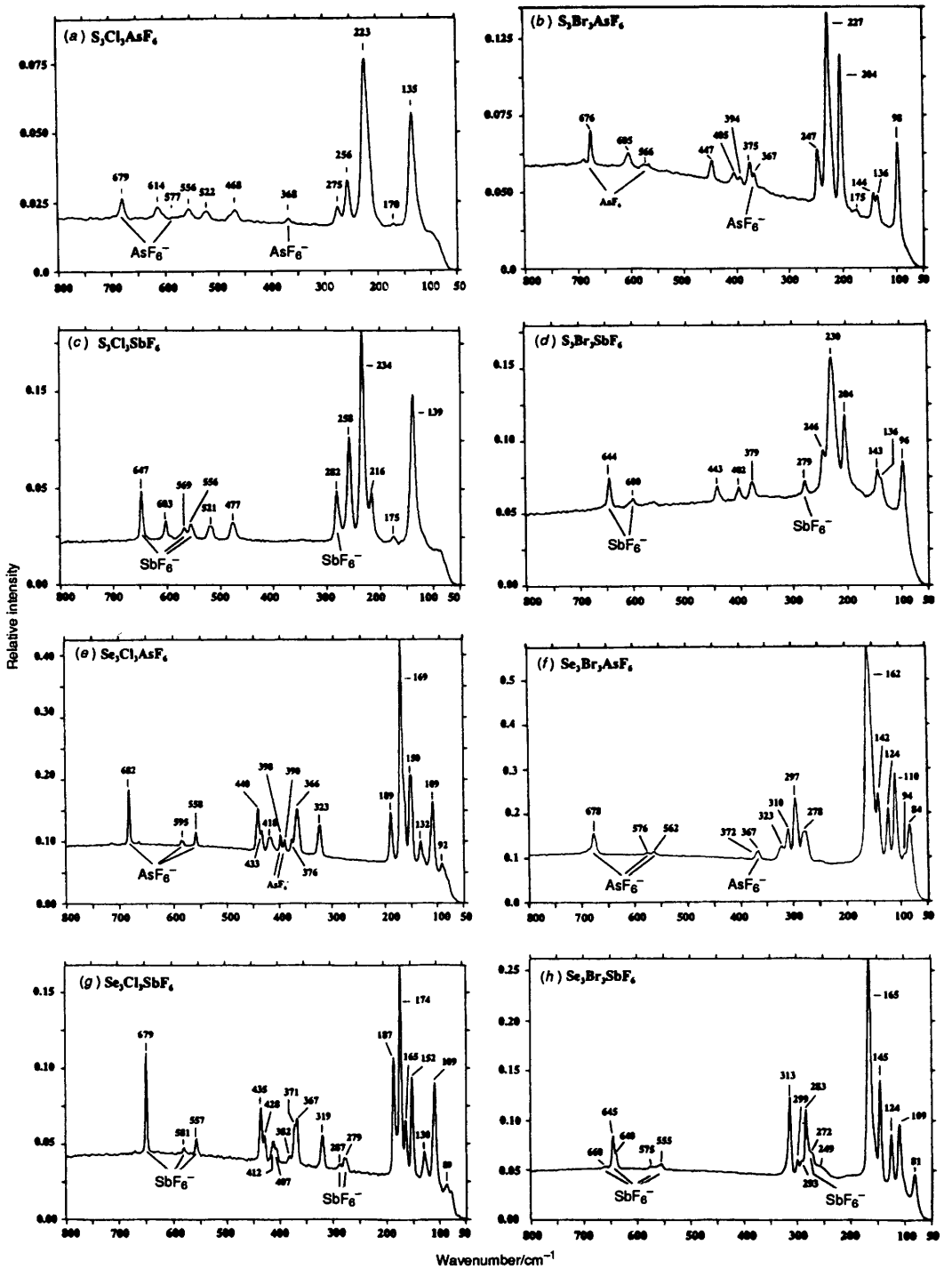

Fig. 6 FT-Raman spectra of the $M_3X_3AsF_6$ and $M_3X_3SbF_6$ salts (resolution 2 cm^{-1}; except for $S_3Cl_3AsF_6$, 4 cm^{-1}). The laser power (mW), temperature (°C) and number of scans are: (*a*) 12, 22, 300; (*b*) 30, −147, 300; (*c*) 22, 22, 256; (*d*) 23, 22, 300; (*e*) 30, −147, 300; (*f*) 30, 22, 600; (*g*) 14, −147, 600; (*h*) 19, −147, 512

estimated bond distances in $S_3Br_3^+$ ($S_3Cl_3^+$) are nearly identical to those obtained from the vibrational data except for the S(3)–Br(3) bond: S(1)–S(2) 2.24 (2.236), S(2)–S(3), 1.935 Å (1.921), S(1)$^+$–X (d_{av}) 2.13 (1.98 Å) and S(3)–X(3) 2.19 (2.05 Å).

Calculation of the geometries and electronic structures of the $M_3Cl_3^+$ cations

In order to understand more fully the nature of the bonding in the $M_3X_3^+$ cations, we carried out RHF/STO-3G* calculations on $Se_3Cl_3^+$, $S_3Cl_3^+$ and $S_3H_3^+$ using the GAUSSIAN 92 suite of computer programs.[20a] The results are shown in Figs. 8 and 9, and Tables 11 and 12. The geometry of the fully optimized structure **I** (calculated at the RHF/STO-3G* level and confirmed at the 6-31G* level for $S_3Cl_3^+$, Fig. 8) is significantly different from that of the observed solid-state structure for $Se_3Cl_3^+$ (**II**, Fig. 8) [*i.e.* there is less bond alternation and no intracation Cl(2)–M(3) contact in **I**]. In addition the energy of the fully optimised structure of $ClS^+(SCl)_2$ [**III**, with a geometry similar to that of $MeS^+(SMe)_2$,[10c] see Fig. 8] is similar to that of **I**, and lower than that with the geometry observed in the solid state. Therefore, the observed geometry of the $M_3X_3^+$ (M = S or Se, X = Cl or Br) cations likely arises, at least in part, from solid-state effects although we cannot rule out the possibility that the optimised gas-phase structure would be identical to that observed in the solid state when computed at a higher level of theory. However, the fact that similar geometries for $S_3Cl_3^+$ were obtained using semiempirical (MNDO) and *ab initio* (LANL1DZ,[20a] STO-3G* and 6-31G* basis sets) calculations suggests this is in fact the correct gas-

Table 9 Sulfur–chlorine and –bromine vibrational frequencies, average S–Cl/S–Br bond distances and angles (°) for different sulfur–chlorine and –bromine compounds (X = Cl or Br)[a,b]

Compound	$\nu(S–X)_{av}/cm^{-1}$	$d(S–X)_{av}/Å$	$X–S–X_{av}/°$	$\delta(X–S–X)_{av}/cm^{-1}$	Ref.
$CF_3SCl_2AsF_6$	550	1.968(2)	104.22(5)	225	56
SCl_3AsF_6	533	1.970	102.3	264	12(*a*)
$MeSCl_2(AsF_6)$	532	1.978(2)	103.2(1)	221	56, 57
SCl_2	516	2.014(5)	102.8 ± 0.2	208	58
$Me(Cl)SSMe(AsF_6)$	514	2.040(3)			59
S_2Cl_2	456	2.057(2)	108.2 ± 0.3	227	58
$O=SCl_2$	473	2.076(6)	96.2 ± 1.0	194	60
$Cl_2SSSClAsF_6$	539 (Cl_2S)	1.97[b]			This work
	468 (SCl)	2.07[b]			
SBr	518	1.997[c]			61
S_7BrAsF_6	416	2.114(16)			6, 15
SBr_3AsF_6	410	2.145(6)	103.8(2)	146	4(*a*), 62
$MeSBr_2(AsF_6)$	410	2.231(4)	107.6(2)	149	63
S_2Br_2	355.5	2.24 ± 0.02	105 ± 3	180	58
$O=SBr_2$	392	2.27 ± 0.02	96.2 ± 1.0	120	60
$Br_2SSSBrAsF_6$	426 (Br_2S)	2.15[b]			This work
	375 (SBr)	2.25[b]			

[a] $\nu(S–X)_{av} = \frac{1}{2}[\nu_{sym}(S–X) + \nu_{asym}(S–X)]$; $\delta(S–X)_{av} = \frac{1}{2}[\delta_{sym}(S–X) + \delta_{asym}(S–X)]$ (possible degeneracy of the vibrations was taken into account). [b] From the S–X (X = Cl or Br) stretching frequencies and the corresponding S–X bond distances the following linear relationships were obtained: $\nu(S–Cl)/cm^{-1} = 1913.90 - 696.54\,d(S–Cl)/Å$ (r −0.90) and $\nu(S–Br)/cm^{-1} = 1432.16 - 468.68\,d(S–Br)/Å$ (r −0.88) (see Fig. 7). [c] Calculated value.[61]

Table 10 Vibrational wavenumbers (cm^{-1}) and bond distances (Å) for different S–S bonds (in the case of sulfur rings the frequencies of equivalent bonds were averaged) in various neutral and cationic compounds containing sulfur–sulfur bonds used to establish the linear relationship. The estimated bond distances for $S_3Cl_3^+$ and $S_3Br_3^+$ are given for comparison

Compound	$\nu(S–S)$	$\bar{\nu}(S–S)$	$d(S–S)$	$\bar{d}(S–S)$	b.o.[a]	Ref.
S_8O	320[b]		2.202[b]		0.5	64
$(C_6F_5S)_2SC_6F_5(AsF_6)$	471	444	2.097(4)	2.088(4)	0.84	11(*a*)
	416		2.080(4)			
$C_6F_5S–SC_6F_5$	489		2.059(4)		0.95	11, 66
S_8O	453[c]		2.056[c]		0.96	64
$MeS(SMe)_2(AsF_6)$	501	478	2.048(3)	2.051(3)	0.99	10(*a*)
(monoclinic)	455		2.054(3)			
S_8	475 (a_1)	457	2.048		1.0	64, 70
	475 (e_2)					
	471 (e_1)					
	437 (e_3)					
	415 (b_1)					
$Me_2SSMe(AsF_6)$	500		2.042(5)		1.02	10(*a*)
Me_2S_2	509		2.022(3)		1.12	67
$Me(MeS)SCl(SbCl_6)$	459		2.004(3)		1.2	59
S_8O	515		2.003		1.2	65
S_2Cl_2	540		1.97		1.4	58
S_2O	679		1.889		1.98	52, 65
S_2F_2	715.0		1.888		2.0	58
$S=SF_2$	760.5		1.86		2.3	58
$S_2I_4(AsF_6)_2$	734.1		1.843(6)		2.4	3, 68
$Cl_2SSSCl(AsF_6)$	614		1.937[d]		1.6	This work
	223		2.246[d]		0.4	
$Br_2SSSBr(AsF_6)$	605		1.944[d]		1.6	This work
	227		2.243[d]		0.4	

[a] Bond orders were calculated according to footnote * on p. 2559. [b] S–S bond adjacent to S=O. [c] Average of two-co-ordinate S–S distances within the ring. [d] Calculated value (see text).

phase configuration. The M–M bond alternation is greater in **IA** [dihedral angle Cl(2)–M(1)–M(2)–M(3) held at 1.2°, all other parameters optimised; see Fig. 8] than in **I**, implying that the bond alternation is enhanced by the X(2) ··· M(3) intracationic contact. However, the bond alternation is still less than that observed in the solid state. In addition, keeping the bond alternation of **II** but allowing all other parameters to optimise leads to **IB** (see Fig. 8), which resembles **I**. This implies that the Cl(2) ··· M(3) intracationic contact is not solely a result of the M–M bond alternation. Forcing the M–M distances to be equal increases the energies of **I** (M = S, 8.0 kJ mol^{-1}) and **II** (M = S, 42.4 kJ mol^{-1}), implying that the stability is increased by bond alternation. Positive charge delocalisation onto M(3) from M(1) increases slightly with bond alternation [*i.e.* **II**: S(1)–S(2) = S(2)–S(3) 2.0 Å, charges S(1) 0.73, S(2) 0.07, S(3) 0.38; geometry with the observed bond alternation, charges S(1) 0.67, S(2) 0.12, S(3) 0.39; for a complete listing see SUP 57126]. However, it is known that charges obtained with this method are not reliable.[71] This analysis is consistent with the valence-bond point of view and implies that the geometry and bond alternation are a result of charge delocalisation from $M(1)^+$ to M(3), the intracationic contact, and also from electrostatic and crystal field effects. Crystal field effects have been shown to be essential in accounting for the long S–S bond in $S_2O_4^{2-}$.[73]

The valence bond model of the bonding in $M_3X_3^+$ is supported by an examination of the molecular orbitals (MOs) (extended Hückel)[19] using the crystal structure geometry of $Se_3Cl_3^+$ [**II** in Table 11 and Figs. (1) and (8)]. A strong bond between Se(2) and Se(3) is reflected in MO 21 [σ] and MOs 17

and 18 [π] (Fig. 10), consistent with some $4p_\pi$–$4p_\pi$ bonding. The very weak Se(1)–Se(2) bond is reflected in the absence of π MOs and presence of weaker σ components relative to Se(2)–Se(3). The weak Cl(2)···Se(3) intracationic interaction is reflected in MO 18, which is weakly bonding between these atoms. Similar results were obtained for the extrapolated crystal structure geometry of $S_3Cl_3^+$. These features are less pronounced or even absent in the MOs of the $S_3Cl_3^+$ and $Se_3Cl_3^+$ cations with the geometries **I** and **IB** shown in Fig. 8. A complete set of MO diagrams for $S_3Cl_3^+$ and $Se_3Cl_3^+$ has been deposited.

The optimised structure of $S_3H_3^+$ (**I**, Fig. 9) is very similar to that of the optimised structure of $M_3Cl_3^+$ (**I**, see Fig. 8), and with an energy almost identical to that of $HS^+(SH)_2$ [**III**, Fig. 9 and which is similar to the geometry of the observed $MeS^+(SMe)_2$[10e]]. The energy difference between structures **I** and **II** for $S_3H_3^+$ (39.8 kJ mol^{-1}) is even higher than for $S_3Cl_3^+$ (26.5 kJ mol^{-1}), consistent with the expected greater strength of the Cl(2)···S(3) intracationic contact relative to that of the H(2)···S(3) intracationic contact and greater charge delocalisation onto the halogen (than hydrogen) adjacent to S^+. The methyl derivative would not be able to make an analogous intracationic contact, and in addition would be severely sterically hindered and therefore is even less likely to adopt the observed Cl_2M^+MMCl solid-state structure (**II**). The relative energies of H_2M^+MMH and $HS^+(H)_2$ [Fig. 9, **I** *versus* **III**, 4.7 kJ mol^{-1}; for $S_3Cl_3^+$ (Fig. 8) **III** is 1.1 kJ mol^{-1} lower than **I**] may change at higher levels of calculation. However, they resemble the $S_3Cl_3^+$ situation, and imply that $M_3H_3^+$ may be prepared from MX_3SbF_6 (M = S,[74] Se) and 2M. Which isomer is formed will probably depend on solid-state stabilisation, but we would not be surprised if it was the H_2M^+ MMH isomer. The theoretical conclusions drawn here are preliminary, and should be viewed as a qualitative interpretation of the bonding trends consistent with the geometries obtained from the X-ray data.

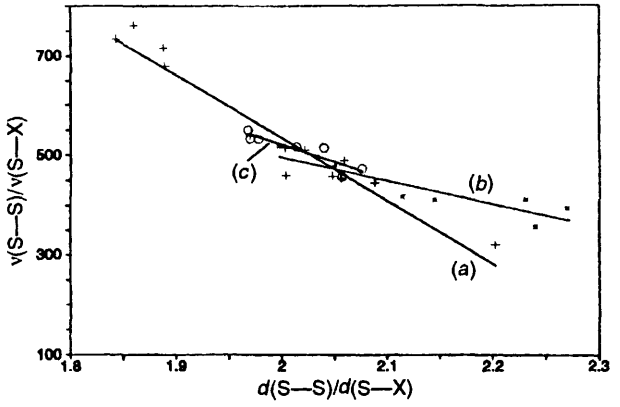

Fig. 7 Linear relationships between (*a*) sulfur–sulfur bond lengths [*d*(S–S)] and stretching frequencies [ν(S–S)], (*b*) sulfur–chlorine bond lengths [*d*(S–Cl)] and stretching frequencies [ν(S–Cl)] and (*c*) sulfur–bromine bond lengths [*d*(S–Br)] and stretching frequencies [ν(S–Br)]. Data are given in Tables 9 and 10

FT-Raman spectrum of $Se_2Br_5AsF_6$

For the $Se_2Br_5^+$ ion **6** with approximately C_{2h} symmetry ($3n - 6$) = 15 fundamental modes of vibration are expected which are either IR or Raman active (mutual exclusion rule for molecules with a centre of symmetry): six stretching, seven bending modes and two torsions.[54] The irreducible representa-

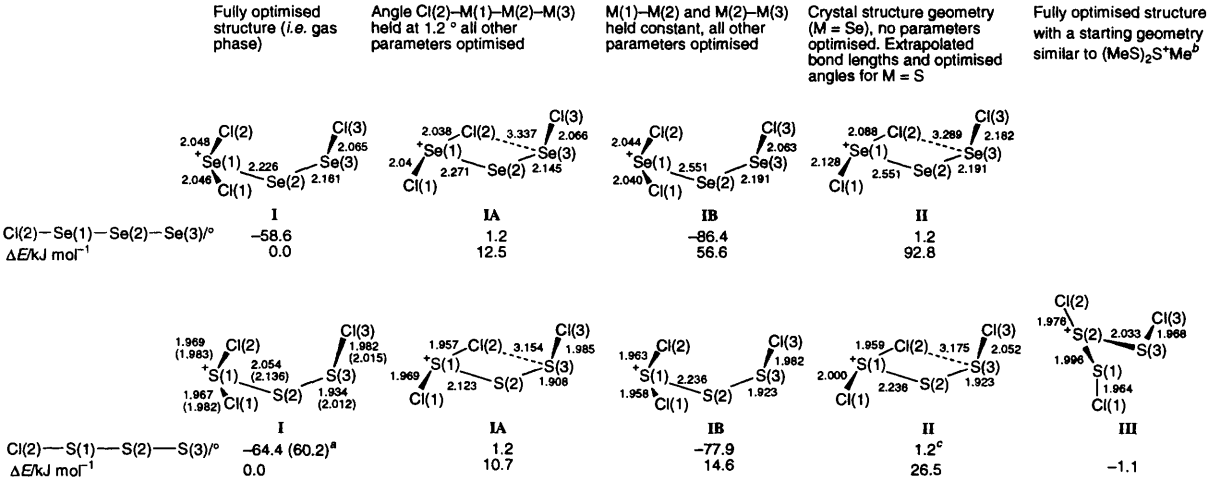

Fig. 8 Calculated structures for $Se_3Cl_3^+$ and $S_3Cl_3^+$. All bond distances in Å. [a] For $S_3Cl_3^+$ (**I**), the numbers in parentheses represent the full geometry optimisation performed at the RHF/6-31G* level. [b] $(MeS)_2S^+Me$ crystal structure, bond distances and dihedral angles:[10e] S(1)–S(2) 1.987, S(2)–S(3) 1.986 Å; C(2)–S(2)–S(3)–C(3) −127, C(1)–S(1)–S(2)–C(2) −69°. $(ClS)_2S^+Cl$ optimised dihedral angles: Cl(2)–S(2)–S(3)–Cl(3) −169 and Cl(1)–S(1)–S(2)–Cl(2) −60°. [c] Dihedral angle Cl(2)–S(1)–S(2)–S(3) held constant at 1.2°

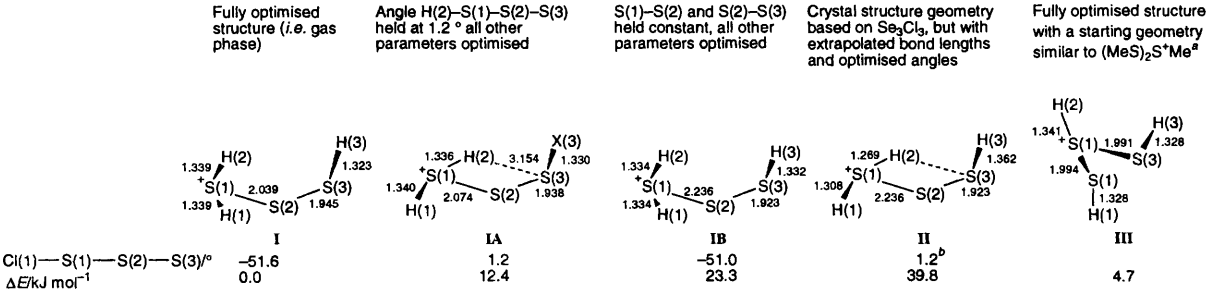

Fig. 9 Calculated structures for $S_3H_3^+$. All bond distances in Å. [a] $(MeS)_2S^+Me$ crystal structure, bond distances and dihedral angles.[10e] $(HS)_2S^+H$ optimised dihedral angles: H(2)–S(2)–S(3)–H(3) −139, H(1)–S(1)–S(2)–H(2) −54° [b] Dihedral angle H(2)–S(1)–S(2)–S(3) held constant at 1.2°

Table 11 Calculated angles (°) for different geometries of $M_3Cl_3^+$ cations (M = S or Se; STO-3G* level). For comparison the experimental data for $Se_3Cl_3^+$ **II** are given. The structures are shown in Fig. 8

	$S_3Cl_3^+$				$(ClS)_2S^+Cl$	$Se_3Cl_3^+$			
Angle	**I**[a]	**IA**	**IB**	**II**[b]	**III**	**I**	**IA**	**IB**	**II**[b]
M(2)–M(3)–Cl(3)	104.0 [105.3]	104.8	105.3	104.1	106.8	102.7	102.8	103.5	104.41(18)
M(1)–M(2)–M(3)	106.0 [108.4]	106.0	104.7	104.6	109.1	104.0	105.0	101.6	102.87(9)
Cl(1)–M(1)–M(2)	104.9 [106.4]	102.9	102.3	101.3	101.8	104.3	102.4	100.6	99.97(15)
Cl(2)–M(1)–M(2)	106.4 [107.3]	104.9	103.3	103.3	—	105.2	104.5	101.3	96.84(16)
Cl(2)–M(1)–Cl(1)	102.6 [103.8]	103.6	103.5	103.5	—	101.3	102.0	102.4	99.77(22)
M(1)–M(2)–M(3)–Cl(3)	80.6 [91.4]	85.8	88.1	86.5	—	90.0	86.9	87.4	87.0(2)
Cl(1)–M(1)–M(2)–M(3)	43.8 [50.4]	109.3	24.4	108.2	—	74.6	107.3	18.7	102.4(2)
Cl(2)–M(1)–M(2)–M(3)	−64.4 [−60.2]	1.2	−77.9	1.2	—	−58.6	1.2	−86.4	1.2(1)
Absolute energy/E_h	−2543.3379 [−2570.5988]					−8 487.0855			
ΔE/kJ mol^{-1}	0.0	10.7	14.6	26.5	−1.1	0.0	12.5	56.6	92.8

[a] **I** represents the fully optimised gas-phase structure (STO-3G*). The results of the 6-31G* calculation for $S_3Cl_3^+$ are given in square brackets. [b] **II** is the crystal structure as determined for $Se_3Cl_3^+$ (AsF_6^- salt). Structure **II** for $S_3Cl_3^+$ is based on the crystal structure as determined for $Se_3Cl_3^+$ (AsF_6^- salt), but with the bond distances extrapolated for S–S and S–Cl as described.

Table 12 Calculated angles (°) for different geometries of $S_3H_3^+$ cations (STO-3G* level). The structures are shown in Fig. 9

	$S_3H_3^+$				$(HS)_2S^+H$
Angle	**I***	**IA**	**IB**	**II***	**III**
S(2)–S(3)–H(3)	97.1	97.4	98.4	104.41	95.4
S(1)–S(2)–S(3)	105.3	104.9	104.8	102.87	111.3
H(1)–S(1)–S(2)	102.4	101.0	98.9	99.97	91.8
H(2)–S(1)–S(2)	102.6	100.4	99.1	96.84	—
H(2)–S(1)–H(1)	93.7	92.7	93.4	93.4	—
S(1)–S(2)–S(3)–H(3)	89.5	89.0	89.5	87.0	—
H(1)–S(1)–S(2)–S(3)	45.1	96.0	43.9	102.4	—
H(2)–S(1)–S(2)–S(3)	−51.6	1.2	−51.0	1.2	—
Absolute energy/E_h	−1181.2359				
ΔE/kJ mol^{-1}	0	12.4	23.3	39.8	4.7

* **I** represents the fully optimised gas-phase structure (STO-3G*). Structure **II** for $S_3H_3^+$ is based on the crystal structure as determined for $Se_3Cl_3^+$ (AsF_6^- salt), but with the bond distances extrapolated for S–S and S–H as described.

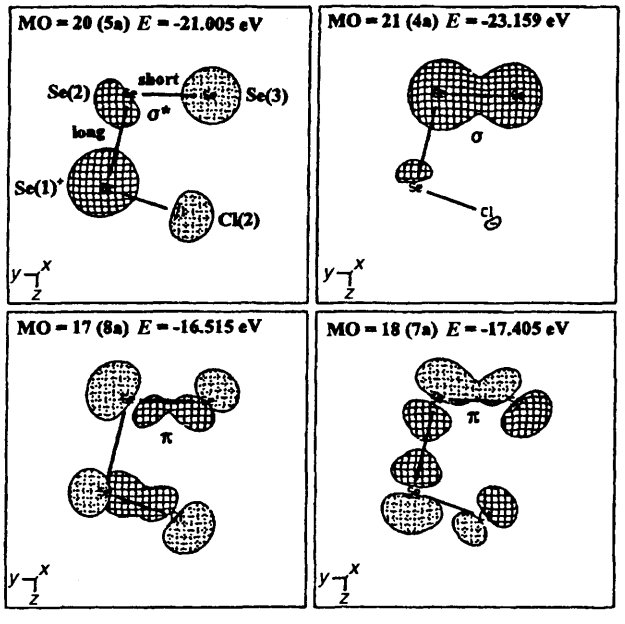

Fig. 10 Selected molecular orbitals (17, 18, 20, 21) for the $Se_3Cl_3^+$ cation generated by extended-Hückel calculations using the crystal structure geometry

tion [54] for the vibrations of the $Se_2Br_5^+$ ion is given in equation (13). The FT-Raman spectrum for $Se_2Br_5AsF_6$ is shown in Fig. 11. The assignments of the six Raman-active modes of the

$$\Sigma_{vib} = 4\,A_g\,(\text{Raman } pol) + 4\,A_u\,(\text{IR}) + 2B_g\,(\text{Raman } depol) + 5\,B_u\,(\text{IR}) \quad (13)$$

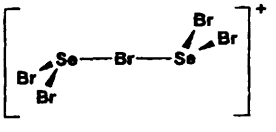

6

$Se_2Br_5^+$ ion (Fig. 11) are based on comparison with known spectra and bond lengths of related species (see Table 6). The two terminal selenium–bromine bond distances in $Se_2Br_5^+$ [2.291(7) and 2.268(6) Å] are comparable to those in the $SeBr_3^+$ cation (see Table 6) where the formal selenium–bromine bond order is *ca.* 1. Therefore, the observed frequencies at 301.4 and 294.1 cm^{-1} belong to the $SeBr_2$ antisymmetric stretch (B_g) and $SeBr_2$ symmetric stretch (A_g), respectively. The vibrational bands at 260 and 119 cm^{-1} are assigned to the $SeBr_2$ wagging and $SeBr_2$ deformation (scissors) by comparison with $OSeBr_2$ (227, 102 cm^{-1}), β-$SeBr_4$ (141 cm^{-1}) and $SeBr_3^+$ (138 cm^{-1}) (see Table 6). The wagging mode is normally expected at higher frequency than that of the scissors mode. The band at the lowest energy is expected to be the $SeBr_2$ twisting mode (B_g) which is found at 84.6 cm^{-1}. The remaining strong band at 160 cm^{-1} is assigned to the SeBr symmetric stretching vibration of the SeBrSe chain by comparison with the related stretching frequency in the Br_3^- ion* and $SeBr_2$(tmtu) (see Table 6).

* Geometry and vibrational frequencies (solid state) observed for the Br_3^- ion in $CsBr_3$ (a) and NEt_4Br_3 (b). Bond distances and angles: (a) 2.440(6), 2.698(6) Å, α = 177.5(2)°; (b) 2.536(2) Å, α = 180°. Raman bands (cm^{-1}): (a) 138 (ν_1, ν_{asym}), 199 and 213 (ν_3, ν_{sym}, shows splitting) and 82 (ν_2, δ); (b) 163 (ν_1, ν_{asym}), 200 (ν_3, ν_{sym}).[72]

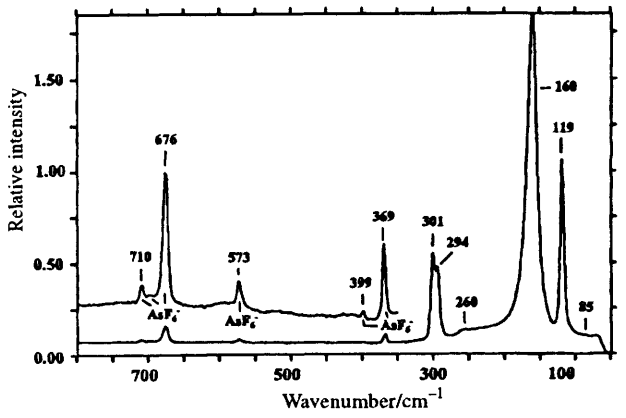

Fig. 11 FT-Raman spectrum of $Se_2Br_5AsF_6$ at 22 °C (laser power 29 mW, 600 scans, resolution 2 cm^{-1}). Expected fundamental vibrations for the $Se_2Br_5^+$ cation with measured wavenumbers (cm^{-1}) and relative intensities in parentheses: A_g (Raman), $\nu_{sym}(SeBr_2)$ 294 (21), $\omega(SeBr_2)$ 260 (1), ν_{sym}(Se–Br–Se) 160 (100), $\delta(SeBr_2$, scissors) 110 (44); A_u (IR) $\nu_{asym}(SeBr_2)$, $\tau(SeBr_2)$ (twisting), $\rho(SeBr_2)$ (rocking), δ(Se–Br–Se) (in plane); B_g (Raman), $\nu_{asym}(SeBr_2)$ 301 (25), $\tau(SeBr_2$, twisting) 85 (< 1); B_u (IR), $\nu_{sym}(SeBr_2)$, $\omega(SeBr_2)$, $\delta(SeBr_2)$ (scissors); δ(Se–Br–Se) (out of plane), ν_{asym}(Se–Br–Se)

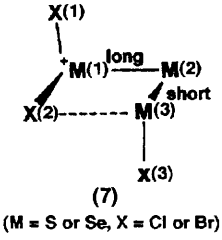

(7)

(M = S or Se, X = Cl or Br)

Conclusion

The salts $M_3X_3AF_6$ (A = As or Sb, M = S or Se, X = Cl or Br) were prepared quantitatively (exception $S_3Br_3SbF_6$, which is non-quantitative) by the reaction of stoichiometric amounts of MX_3AF_6 and chalcogen in sulfur dioxide solution at room temperature according to equation (1). The salt $M_3Br_3AsF_6$ was also prepared quantitatively from stoichiometric quantities of chalcogen, bromine, and arsenic pentafluoride. Attempts to prepare $M_3X_3AF_6$ containing both sulfur and selenium, $M_xX_3AF_6$ (x = 2 or 4) as well as $S_3Cl_3AlCl_4$ were unsuccessful. The $M_3X_3^+$ cations are of interest in their own right as simple binary sulfur- and selenium–halogen species and as they are the smallest cations in which chalcogen–chalcogen bond alternation can occur, a common feature of the more complex family of polychalcogen–halogen cations.[1a,8,18]

The crystal structures of the $M_3X_3AsF_6$ salts were determined. All contained $(X_2MMMX)^+$ cations although the sulfur cations were disordered. However, the FT-Raman spectra showed that all cations had similar structures, and bond distances were estimated for the sulfur cations from the vibrational data. The ^{77}Se FT-NMR spectrum of $Se_3Br_3^+$, in sulfur dioxide solution at low temperatures, showed three distinct selenium environments suggesting retention of the structure. The cations adopt X_2M^+MMX structures **7**, in contrast to the symmetrical $RM^+(MR)_2$ (R = Me or C_6F_5),[10,11a] have pronounced chalcogen–chalcogen bond alternation {$S_3Cl_3^+$ [$S_3Br_3^+$], estimated: S(1)–S(2), 2.246 [2.243] and S(2)–S(3), 1.937 [1.944] Å; $Se_3Cl_3^+$ [$Se_3Br_3^+$], X-ray: Se(1)–Se(2), 2.551(3) [2.558(6)] and Se(2)–Se(3), 2.191(3) [2.207(6)] Å} and chalcogen–halogen intercation contacts. The shorter of the chalcogen bonds have bond orders greater than 1 {S(2)–S(3) b.o.: 1.6 [$S_3Cl_3^+$], 1.6 [$S_3Br_3^+$]. Se(2)–Se(3) b.o.: 1.7 [$Se_3Cl_3^+$], 1.6 [$Se_3Br_3^+$]} indicative of the presence of thermodynamically stable $3p_\pi$–$3p_\pi$ and $4p_\pi$–$4p_\pi$ bonds, and as far as we are aware the Se–Se bonds are the shortest so far observed in an isolated compound. We propose that the bond alternation arises from positive-charge delocalisation from M(1) to M(3) with the valence-bond structures **3** as well as **4** making a significant contribution to the bonding in the cation. This view is supported by the results of *ab initio* calculations (RHF/STO-3G*) which also imply that the bond alternation is enhanced by both the M(3)···X(2) intracationic contact and solid-state effects (lattice energies, cation–cation and –anion effects). The importance of the crystal field in accounting for long S–S bond lengths has been shown for $S_2O_4^{2-}$.[73] It is not possible to make a similar intracationic contact when X = Me[10a,c] or C_6F_5[11a] and consistently $XM^+(MX)_2$ structures are adopted for these derivatives.

Before this work the chemistry of polychalcogen–halogen cations was largely restricted to that of sulfur- and selenium–iodine cations.[1a,18] Based on the relative stabilities of S_7I^+[1,2a,c] and S_7Br^+[6] we anticipated that the chemistry of the poly-sulfur and -selenium chlorine/bromine cations would be very restricted. However, the isolations of the $M_3X_3^+$ salts [Se_9Cl^+][14] and $Se_2Br_5^+$ (see ref. 7, FT-Raman spectrum assigned see above) have also been characterised] suggest this may not be the case.

Acknowledgements

We thank the Natural Sciences and Engineering Research Council of Canada for an operating grant (to J. P., T. S. C.), a Graduate Fellowship (to S. B.) and an International Postdoctoral Fellowship (to G. S.) and the Donors of The Petroleum Research Fund (J. P.), administered by the American Chemical Society. In addition, we thank M. Tajik for his preliminary investigations, Drs. F. Grein and P. Bruna for their assistance with the *ab initio* calculations, Dr. P. Penner for his support in obtaining the FT-NMR data on the Unity 400 Varian spectrometer, and Drs. P. D. Boyle and P. S. White for solving the crystal structures of $Se_3Cl_3AsF_6$ and $S_3Br_3AsF_6/Se_3Br_3AsF_6$, respectively.

References

1 (*a*) T. Klapötke and J. Passmore, *Acc. Chem. Res.*, 1989, **22**, 234 and refs. therein; (*b*) J. Passmore, G. W. Sutherland, P. Taylor, T. K. Whidden and P. S. White, *Inorg. Chem.*, 1981, **20**, 3839; J. Passmore, P. Taylor, T. K. Whidden and P. S. White, *J. Chem. Soc., Chem. Commun.*, 1976, 689.

2 J. Passmore, G. W. Sutherland and P. S. White, (*a*) *Inorg. Chem.*, 1982, **21**, 2717; (*b*) *J. Chem. Soc., Chem. Commun.*, 1979, 901; (*c*) *J. Chem. Soc., Chem. Commun.*, 1980, 330.

3 (*a*) M. P. Murchie, J. P. Johnson, J. Passmore, G. W. Sutherland, M. Tajik, T. K. Whidden, P. S. White and F. Grein, *Inorg Chem.*, 1992, **31**, 273; (*b*) W. A. S. Nandana, J. Passmore, P. S. White and C.-M. Wong, *Inorg. Chem.*, 1990, **29**, 3529.

4 (*a*) J. Passmore and P. Taylor, *J. Chem. Soc., Dalton Trans.*, 1976, 804; (*b*) J. P. Johnson, M. P. Murchie, J. Passmore, M. Tajik, P. S. White and C.-M. Wong, *Can. J. Chem.*, 1987, **65**, 2744.

5 W. A. S. Nandana, J. Passmore, P. S. White and C.-M. Wong, *Inorg. Chem.*, 1989, **28**, 3320.

6 J. Passmore, G. W. Sutherland, T. K. Whidden, P. S. White and C.-M. Wong, *Can. J. Chem.*, 1985, **63**, 1209.

7 M. P. Murchie, J. Passmore and P. S. White, *Can. J. Chem.*, 1987, **65**, 1584.

8 J. Beck, *Angew. Chem., Int. Ed. Engl.*, 1994, **33**, 163; *Chem. Ber.*, 1995, **128**, 23.

9 R. Faggiani, R. J. Gillespie and J. W. Kolis, *J. Chem. Soc., Chem. Commun.*, 1987, 592.

10 (*a*) R. Minkwitz, V. Gerhard, R. Krause, H. Prenzel and H. Preut, *Z. Anorg. Allg. Chem.*, 1988, **559**, 154; (*b*) R. Minkwitz, R. Krause, H. Prenzel and H. Preut, *Z. Anorg. Allg. Chem.*, 1989, **571**, 133; (*c*) R. Laitinen, R. Steudel and R. Weiss, *J. Chem. Soc., Dalton Trans.*, 1986, 1095; (*d*) H. Meerwein, K. F. Zenner and R. Gipp, *Liebigs Ann. Chem.*, 1965, **688**, 67; (*e*) R. Minkwitz, H. Prenzel and H. Pritzkow, *Z. Naturforsch., Teil. B*, 1987, **42**, 750.

11 (*a*) J. Passmore, G. Schatte and G. W. Sutherland, *Can. J. Chem.*, 1996, in the press; (*b*) J. Passmore, E. K. Richardson and P. Taylor, *J. Chem. Soc., Dalton Trans.*, 1976, 1006.

12 (*a*) R. Minkwitz, K. Jänichen, H. Prenzel and V. Wölfel, *Z. Naturforsch., Teil B*, 1985, **40**, 53 and refs. therein; (*b*) R. Minkwitz and V. Gerhard, *Z. Naturforsch., Teil B*, 1989, **44**, 364; (*c*) R. Minkwitz, A. Kornath and H. Preut, *Z. Naturforsch., Teil B*, 1992, **47**, 594 and refs. therein.
13 Gmelin, *Handbook of Inorganic Chemistry, Selenium, Suppl.*, 8th edn., vol. B2, Springer, Berlin, 1984 and refs. therein.
14 R. Faggiani, R. J. Gillespie, J. W. Kolis and K. C. Malhotra, *J. Chem. Soc., Chem. Commun.*, 1987, 591.
15 R. Minkwitz and J. Nowicki, *Inorg. Chem.*, 1990, **29**, 2361.
16 A. Bali and K. C. Malhotra, *Aust. J. Chem.*, 1975, **28**, 983; *J. Inorg. Nucl. Chem.*, 1977, **39**, 957.
17 W. Sawodny and E. Rost, *Z. Anorg. Allg. Chem.*, 1990, **586**, 19.
18 J. Passmore, in *Studies in Inorganic Chemistry*, ed. R. Steudel, Elsevier, New York, 1992, vol. 14, ch. 19, p. 373 and refs. therein.
19 C. Mealli and D. M. Proserpio, *J. Chem. Educ.*, 1990, **67**, 399.
20 (*a*) Los Alamos National Laboratories 1 Double Zeta: P. J. Hay and W. R. Wadt, *J. Chem. Phys.*, 1985, **82**, 270; 284; 299; (*b*) M. J. Frisch, G. W. Trucks, H. B. Schlegel, P. M. W. Gill, B. G. Johnson, M. W. Wong, J. B. Foresman, M. A. Robb, M. Head-Gordon, E. S. Replogle, R. Gomperts, J. L. Andres, K. Raghavachari, J. S. Binkley, C. Gonzalez, R. L. Martin, D. J. Fox, D. J. Defrees, J. Baker, J. J. P. Stewart and J. A. Pople, GAUSSIAN 92/DFT (486-Windows-G92/DFT-Revision G.3), Gaussian, Inc., Pittsburgh, PA, 1993.
21 J. Passmore, M. Tajik and P. S. White, *J. Chem. Soc., Chem. Commun.*, 1988, 175.
22 P. Bakshi, P. D. Boyle, T. S. Cameron, G. Schatte and G. W. Sutherland, *Inorg. Chem.*, 1994, **33**, 3849; P. D. Boyle, T. S. Cameron, J. Passmore, G. Schatte and G. W. Sutherland, *J. Fluorine Chem.*, 1995, **71**, 217.
23 M. P. Murchie, R. Kapoor, J. Passmore and G. Schatte, *Inorg. Synth.*, 1996, **31**, 80.
24 (*a*) J. Passmore, E. R. Richardson, T. K. Whidden and P. S. White, *Can. J. Chem.*, 1980, **58**, 851 and refs. therein; (*b*) P. D. Boyle, T. S. Cameron, J. Passmore, G. Schatte and T. C. Way, *Can. J. Chem.*, 1996, in the press.
25 M. J. Collins, R. J. Gillespie, J. F. Sawyer and G. J. Schrobligen, *Inorg. Chem.*, 1986, **25**, 2053; R. C. Burns, M. J. Collins, R. J. Gillespie and G. J. Schrobligen, *Inorg. Chem.*, 1986, **25**, 4465.
26 W. A. S. Nandana, J. Passmore and P. S. White, *J. Chem. Soc., Dalton Trans.*, 1985, 1623.
27 (*a*) TEXSAN, Crystal Structure Analysis Package, Molecular Structure Corporation, Houston, TX, 1985, 1992; (*b*) N. Walker and D. Stuart, *Acta Crystallogr., Sect. A*, 1983, **39**, 158.
28 E. J. Gabe, Y. Le Page, J. P. Charland, F. L. Lee and P. S. White, *J. Appl. Crystallogr.*, 1989, **22**, 384.
29 G. M. Sheldrick, SHELXS 86, in *Crystallographic Computing*, eds. G. M. Sheldrick and C. Goddard, Oxford University Press, Oxford, 1985, pp. 175–189.
30 G. M. Sheldrick, SHELX 76, Program for Crystal Structure Determination, University of Cambridge, 1976.
31 D. T. Cromer and J. T. Waber, *International Tables for X-Ray Crystallography*, Kynoch Press, Birmingham, 1974, vol. 4, Table 2.2.4.
32 D. T. Cromer, *International Tables for X-Ray Crystallography*, Kynoch Press, Birmingham, 1974, vol. 4, Table 2.3.1.
33 (*a*) D. A. Johnson, *Some Thermodynamic Aspects of Inorganic Chemistry*, 2nd edn., Cambridge University Press, Cambridge, 1982; (*b*) W. E. Dasent, *Inorganic Energetics*, 2nd edn., Cambridge University Press, Cambridge, 1982; (*c*) R. Laitinen and T. Pakkanen, *J. Mol. Struct.*, 1983, **91**, 337; (*d*) J. Drowart and S. Smoes, *J. Chem. Soc., Faraday Trans. 2*, 1977, 1755.
34 N. N. Greenwood and A. Earnshaw, *Chemistry of the Elements*, Pergamon, Oxford, 1984.
35 J. D. Dunitz, V. Schomaker and K. N. Trueblood, *J. Phys. Chem.*, 1988, **92**, 856 and refs. therein.
36 A. Bondi, *J. Phys. Chem.*, 1964, **68**, 441.
37 V. Schomaker and D. P. Stevenson, *J. Am. Chem. Soc.*, 1941, **63**, 37.
38 L. Pauling, *The Nature of the Chemical Bond*, 3rd edn., Cornell University Press, Ithaka, NY, 1960.
39 I. D. Brown, in *Structure and Bonding in Crystals*, eds. M. O'Keefe and A. Navrotsky, Academic Press, London, 1981, vol. 2, p. 1.
40 S. C. Nyburg and C. H. Faerman, *Acta Crystallogr., Sect. B*, 1985, **41**, 274.
41 G. Gafner and G. J. Kruger, *Acta Crystallogr., Sect. B*, 1974, **30**, 250.
42 P. Cherin and P. Unger, *Acta Crystallogr., Sect. B*, 1972, **28**, 313.
43 C. F. Campana, F. Y.-K. Lo and L. F. Dahl, *Inorg. Chem.*, 1979, **18**, 3060 and refs. therein.
44 A. H. Cowley, *Acc. Chem. Res.*, 1984, **17**, 386; M. W. Schmidt, P. N. Truong and M. S. Gordon, *J. Am. Chem. Soc.*, 1987, **109**, 5217.
45 M. Broschag, T. M. Klapötke, I. C. Tornieporth-Oetting and P. S. White, *J. Chem. Soc., Chem. Commun.*, 1992, 1390.
46 W. V. F. Brooks, J. Passmore and E. K. Richardson, *Can. J. Chem.*, 1979, **57**, 3230.
47 R. Steudel and D. Jensen, *Polyhedron*, 1990, **9**, 1199.
48 K. J. Wynne, P. S. Pearson, M. G. Newton and J. Golen, *Inorg. Chem.*, 1972, **11**, 1192.
49 N. Burford, J. Passmore and J. C. P. Sanders, *From Atoms to Polymers, Isoelectronic Analogies*, eds. J. F. Liebman and A. Greenberg, VCH, New York, 1989, ch. 2, p. 53.
50 M. M. Carnell, F. Grein, M. P. Murchie, J. Passmore and C.-M. Wong, *J. Chem. Soc., Chem. Commun.*, 1986, 225.
51 G. M. Begun and A. C. Rutenberg, *Inorg. Chem.*, 1967, **6**, 2212.
52 R. Steudel, *Spectrochim. Acta, Part A*, 1975, **31**, 1065.
53 I. Dionne, G. Schatte and J. Passmore, unpublished work.
54 N. B. Colthup, L. H. Daly and S. B. Wiberley, *Introduction to Infrared and Raman Spectroscopy*, Academic Press, London, 1984.
55 K. Nakamoto, *Infrared and Raman Spectra of Inorganic and Coordination Compounds*, 4th edn., Wiley, New York, 1986.
56 R. Minkwitz, U. Nass, A. Radünz and H. Preut, *Z. Naturforsch., Teil B*, 1985, **40**, 1123.
57 R. Minkwitz, V. Gerhard and H. Preut, *Z. Anorg. Allg. Chem.*, 1990, **580**, 115.
58 Gmelin, *Handbook of Inorganic Chemistry, Schwelfelhalogenide, Erg.-Bd. 2*, 8th edn., Springer, Berlin, 1978 and refs. therein.
59 R. Minkwitz, A. Kornath, R. Krause and H. Preut, *Z. Naturforsch., Teil B*, 1990, **45**, 1637.
60 Gmelin, *Handbook of Inorganic Chemistry, Thionylhalogenide, Erg.-Bd. 1*, 8th edn., Springer, Berlin, 1978 and refs. therein.
61 M. Feuerhahn, R. Minkwitz and G. Vahl, *Spectrochim. Acta, Part A*, 1980, **36**, 183.
62 J. Passmore, E. K. Richardson and P. Taylor, *Inorg. Chem.*, 1978, **17**, 1681.
63 R. Minkwitz, H. Prenzel, A. Werner and H. Preut, *Z. Anorg. Allg. Chem.*, 1988, **562**, 42.
64 R. Steudel, *Z. Naturforsch., Teil B*, 1975, **30**, 281; R. Steudel and D. F. Eggers, jun., *Spectrochim. Acta, Part A*, 1975, **31**, 871.
65 E. H. Fink, H. Kruse and D. A. Ramsay, *J. Mol. Spectrosc.*, 1986, **119**, 377.
66 C. M. Woodard, D. S. Brown, J. D. Lee and A. G. Massey, *J. Organomet. Chem.*, 1976, **121**, 333.
67 (*a*) S. G. Frankiss, *J. Mol. Struct.*, 1969, **3**, 89; (*b*) B. Beagley and K. T. McAloon, *Trans. Faraday Soc.*, 1971, **67**, 3216.
68 S. Brownridge, J. Passmore and G. Schatte, unpublished work.
69 R. Steudel, *Angew. Chem., Int. Ed. Engl.*, 1975, **14**, 655.
70 P. Coppens, Y. W. Yang, R. H. Blessing, W. F. Cooper and F. K. Larsen, *J. Am. Chem. Soc.*, 1977, **99**, 760.
71 S. Fliszár and H. Dugas, *J. Am. Chem. Soc.*, 1974, **96**, 4358.
72 G. R. Burns and R. M. Renner, *Spectrochim. Acta, Part A*, 1991, **47**, 991; G. R. Burns and R. J. H. Clark, *J. Phys. Chem. Solids*, 1986, **47**, 1049.
73 K. L. Carter, J. B. Weinrach and D. W. Bennett, *J. Am. Chem. Soc.*, 1993, **115**, 10 981.
74 K. O. Christie, *Inorg. Chem.*, 1975, **14**, 2230.

Received 1*st August* 1995; *Paper* 5/05128B